Investigating mechanical properties of a protein by single molecule atomic force microscopy

by

TAO SHEN

A THESIS SUBMITTED IN PARTIAL FULFILLMENT OF
THE REQUIREMENTS FOR THE DEGREE OF

MASTER OF SCIENCE

in

The Faculty of Graduate Studies
(Chemistry)

THE UNIVERSITY OF BRITISH COLUMBIA
(Vancouver)

May 2012

Abstract

Single molecule AFM is a powerful technique affording the opportunity to understand the mechanical properties of proteins at the level of a single molecule. In Combining with the protein engineering techniques, single molecule allows us to understand protein folding/unfolding mechanisms and develop methods to tune the mechanical stability. Here, we use a small protein, GB1, the B1 IgG binding domain of protein G from Streptococcus, as a model system. In this thesis, we employed bi-His metal binding sites to probe the mechanical unfolding transition state of GB1 and rationally enhance the mechanical stability of GB1 mutant, G6-53.

The transition state cannot be trapped and detected by the usual structural methods because of its high free energy. It remains a challenging task and research focus. In Chapter 3, we directly probed the mechanical unfolding transition state structure of protein GB1. The results demonstrate that the contacts between the force-bearing strands 1 and 4 are largely disrupted at the transition state, whereas the first β-hairpin and α-helix were largely intact. The second hairpin was partially disrupted. These results are in close agreement with, and provide a benchmark for, MD simulations.

The mechanical stability is critical for the overall mechanical properties of elastomeric proteins. Elastomeric proteins provide tissues with extensibility, elasticity, and mechanical strength. In Chapter 4, we enhanced the mechanical stability of G6-53 with different metal ions. We demonstrated that all four divalent metal ions, Ni^{2+}, Co^{2+}, Zn^{2+} and Cu^{2+}, enhance the mechanical stability of G6-53 to different degrees. Because this process is completely reversible, the protein can be treated like a switch. Moreover, the

resultant unfolding force difference between Co^{2+} and Zn^{2+} or Zn^{2+} and Cu^{2+} is ~ 20 pN. Thus, various metal ions can be used to fine tune the mechanical stability of proteins.

Table of Contents

List of Tables

List of Figures

Acknowledgements

I would like to give special thanks to my supervisor, Dr. Hongbin Li, for his support and patience throughout this work. His expertise and dedication to research have inspired me to be passionate about my research. Thank you to all the past and present lab-mates. You guys are so kind and patient to me. I am grateful for the time and assistance you guys provided me.

I would like to acknowledge the faculty and staff at UBC for their help, especially Jessie and Elena at Bioservices, who trained me to use the instruments in the bioservices lab.

Finally, I would like to thank my parents, without whose love and encouragement none of this would have been possible.

Chapter 1: Introduction

1.1 Single molecule atomic force microscopy

1.1.1 Origin and development of the atomic force microscopy

In 1981, Binnig and Rohrer from the IBM research laboratory invented the scanning tunnelling microscopy (STM). STM is based on the electron tunnelling effect. When two conductors are close enough, electron will tunnel through the potential barrier and form a tunnelling current. The tunnelling current increases exponentially as the distance between the two conductor decreases. STM measures the tunnelling current and maintains it at a constant level by moving the tip up and down, so that the tip can map the sample height when scanning the surface. Binnig and Rohrer received the Nobel Prize in Physics in 1986 for inventing STM, a fundamental advancement in imaging technology. However, STM is limited to the conductive surface, a limitation that led to the development of Atomic force microscopy (AFM) by Binnig, Quate and Gerber in 1986[1].

As AFM is designed to overcome the limitation of STM, AFM was originally used to probe the surface of samples. A silicon or silicon nitride cantilever with a sharp tip at the end is used to scan the specimen surface. When the cantilever is brought to the surface, the tip moves up and down according to the contour of the sample. The movement of the tip causes the cantilever assembly to deflect. The deflection is measured by a laser beam reflecting from the top surface of the cantilever assembly onto a photodiode detector. In

1987, Marti et al. demonstrated that AFM could be used in a liquid system[2]. It was of major importance that this technology could be applied to biological systems. In 1994, Florin et al. revealed that AFM can directly measure the unbinding force of a single avidin-biotin interaction[3]. This was a milestone for AFM technology. Since then, AFM has been used to not only as an imaging system but also as a force spectroscopy tool. In recent years, polysaccharide, DNA and polyprotein have been studied extensively using AFM[4-10].

1.1.2 Different biomolecules studied using AFM

1.1.2.1 Polysaccharide

After the successful force measurement of the unbinding force of avidin and biotin, Polysaccharide was the first single biomolecule studied using the force-measuring mode AFM[5]. Polysaccharides are of interest to researchers because of their key storage and structure roles in living organisms. In 1997, Rief et al. measured the extension of dextran as a function of applied force. Dextran is composed of glucose monomers which are linked by their C1 carbon atoms and the C6 carbon atoms form the neighbour glucose. Dextran was immobilized at the gold substrate in the experiment. Stretching the dextran produced a typical shoulder at about force 700 pN. The force was kept constant while the dextran extension length increased. The molecular dynamics simulation indicated that the shoulder in the force-extension curve of the dextran resulted from the orientation change of the O-glycosidic bond. The deformation caused every glucose monomer to extended

10 percent. Merszalek et al. demonstrated that amylose exhibits a similar transition[11]. In amylose, glucose monomers are linked between C1 carbon atom and neighbour C4 carbon atoms. Molecular modeling suggests that the transition is from a chair to a twisted-boat conformation change. To further support this hypothesis, Merszalek et al. utilized periodate to cleave the polysaccharide ring in amylose. When the polysaccharide ring was broken, the shoulder in the force-extension curve disappeared. This result confirmed the influence of the polysaccharide ring conformation change on the elasticity behaviour of polysaccharide.

1.1.2.2 DNA

As is well known, DNA plays an important role in the storage, duplication and transcription of genetic information. In living organisms, DNA usually forms a double helix structure. DNA has been extensively studied initially using optical tweezers and later AFM[12, 13]. Optical tweezers are one type of force spectroscopy. When λ-phage DNA is stretched using Optical tweezers, there is a highly cooperative transition at 65 pN. Native dsDNA is converted from B conformation to an overstretched S conformation, called a B-S transition. During this transition, the length of a DNA helix increases significantly, extending by 1.5-2 times its native length. The advantage of AFM over optical tweezers is that the former can investigate systems in the nanonewton range whereas the latter are limited to the 100 pN range. The Gaub group employed AFM to extend λ-phage DNA[14]. Besides the B-S transition at 65 pN, there was a second transition indicated by a shoulder at a higher force of around 150 pN. This shoulder is called the melting transition. During this new transition, the dsDNA is split into two single strands.

The researchers found that both of the B-S and melting transitions were sequence dependent, when they constructed a double-stranded poly (dG-dC) and poly (dA-dT). For the poly (dG-dC) the force at the B-S transition was the same as that of the λ-phage DNA. However, it was also found that the melting force had shifted to approximately 300 pN. For the poly (dA-dT), the B-S transition force was reduced to 35 pN, and the strands started to melt during this process. Thus no melting transition could be observed.

1.1.2.3 Protein

The first study of a single molecule protein with AFM was conducted by Rief et al[15]. Many native proteins perform their biological function under a mechanical load. There is a fundamental difference between proteins unfolded by force as exposed to a chemical denaturant or heat. Thus, proteins' mechanical properties can not be investigated through chemical or thermo analysis. The Gaub group stretched a giant muscle protein called titin, which is responsible for the passive tension developed by muscles. It consists of 244 repeats of Ig-like and fibronectin-like domains, each of which forms a seven –stranded β-barrel structure. The stretching of native titin produced a sawtooth-like curve. The maximum force of the peaks ranged from 150 pN to 300 pN; the peaks were spaced 25 to 28 nm. Each peak corresponded to the unfolding events of one domain in the native titin. It was the first time that the mechanical stability of a single molecule of protein had been investigated. Since then, AFM's excellent spatial resolution (angstroms), high force sensitivity (piconewtons) and large force range (from ~5 pN to ~10nN) have made it a powerful instrument for studying protein folding mechanisms and protein mechanical stability. In this thesis, AFM will be used to investigate a single polyprotein molecule.

1.1.3. Overview of the atomic force microscopy

1.1.3.1 Principles of single molecule atomic force microscopy

Figure 1.1 below shows the basic AFM assembly in a force-measuring mode. The four main components consist of a piezoelectric positioner, an optical detection system, a fluid cell containing a silicon nitride cantilever assembly, a vibration isolation system. A protein solution is adsorbed onto a substrate which is typically a glass coverslip. The substrate is attached to the piezoelectric positioner. When the cantilever is brought into contact with the substrate, the protein is picked up by the cantilever. In this way, a protein bridge is formed between the cantilever and the substrate. The protein can be stretched or relaxed by moving the positioner away or toward the tip. As the protein is stretched, the mechanical force is determined by the cantilever assembly. The cantilever assembly can be regarded as a spring. Thus, the force applying on the cantilever is given by Hook's law:

$$F = k_c \Delta z_c \tag{1.1}$$

where F represents the force, k_c and Δz_c the spring constant and cantilever deflection, respectively. The extension of the molecule E_x is calculated from the movement of the piezoelectric positioner Δz_p and the deflection of the cantilever Δz_c:

$$E_x = \Delta z_p - \Delta z_c \tag{1.2}$$

The deflection of the cantilever Δz_c is monitored by the optical deflection system. The vibration isolation system is used to reduce external noise.

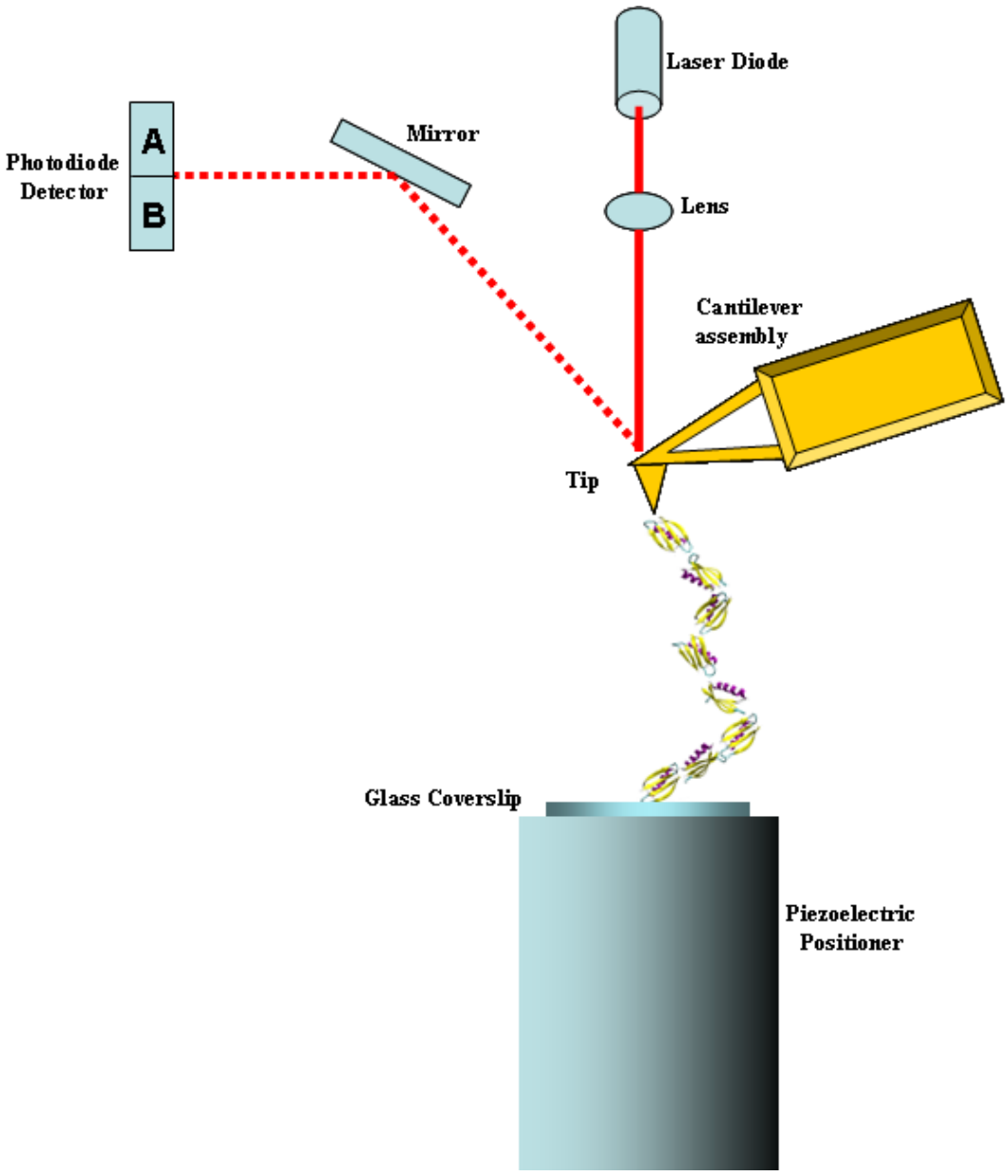

Figure 1.1 Schematic of a single molecule AFM assembly. The polyprotein is adsorbed onto a clean glass coverslip mounted onto a piezoelectric positioner. The polyprotein is picked up randomly by the cantilever tip. The protein can be stretched or relaxed by moving the positioner away or toward the tip. The force applied to the polyprotein is determined from the deflection of the cantilever assembly which is monitored by the movement of the laser spot on the photodiode. The extension of the molecule is detected by the position of the piezoelectric positioner and deflection of the cantilever assembly. Typically the top surface of the cantilever is coated with gold to enhance reflectivity.

1.1.3.2 Piezoelectric positioner

In the force model, AFM requires accurate force and extension measurements. Thus, the piezoelectric positioner is an important component of the AFM assembly. First, it is the source of applied force. When the positioner is moved away from the cantilever, the protein between the substrate and cantilever is stretched and inducing a mechanical force. Second, the extension of a single molecule protein is measured, in part, by its position. The scale of the elongation of a single protein molecule is in the nanometer range. The piezoelectric positioner has an ultra high special resolution along the z-axis. The ultra precise movement of the positioner is essential in single molecule studies.

1.1.3.3 The AFM head and optical detection system

The AFM head includes the laser diode and a position-sensitive photodiode. The laser diode and photodiode constitute the optical detection system. The photodiode, which is divided into upper and lower segments, converts incident light into voltage. The voltage difference between the two sections indicates the deflection of the cantilever. The laser diode produces a laser beam, which is focused on the end of cantilever assembly. The aligning process utilizes the integrated CCD camera. By the camera, the position of laser beam can be visualized on the screen. On the top of the AFM head are two laser-adjusting screws used to adjust the laser beam position in the X-Y plane. The laser-adjusting screws are adjusted until the laser light is focused on the end of the cantilever assembly. The reflected laser beam is reflected onto the photodiode by a tilt mirror. There

are also two photodiode-adjusting screws which adjust the reflecting light onto the center of photodiode. At this point the laser beam is calibrated and the voltage difference is zero.

When the cantilever is deflected, the voltage difference is observed as the laser beam position changes. To convert the voltage output to a measure of the deflection, it is necessary to determine the ratio $\Delta V / \Delta z_c$. To determine this ratio, the positioner is raised until it makes contact with the cantilever assembly, the deflection of the cantilever is equal to the piezoelectric positioner movement. The movement of the positioner produces a linear voltage vs. the deflection response. The slope of the graph below is used to calculate the cantilever deflection from the voltage output.

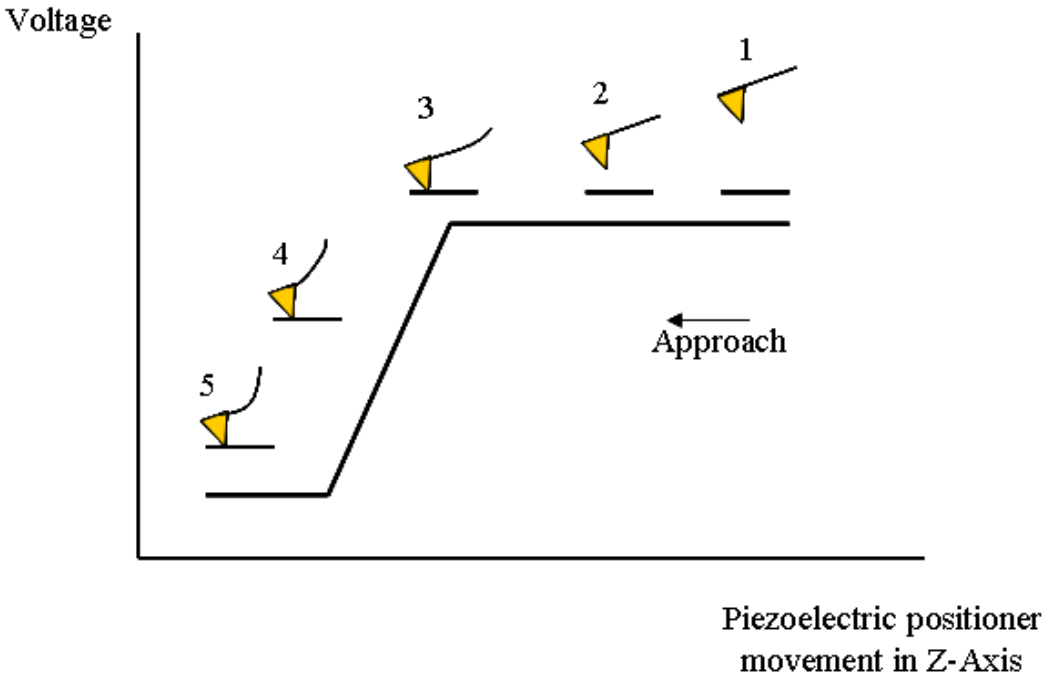

Figure 1.2 The voltage difference versus the cantilever deflection ratio determination. The positioner is raised to the cantilever assembly (stage 1 to stage 2) until the tip and the positioner are adhered to each other (stage 3). When keeping moving the positioner, the deflection of the cantilever is equal to the piezoelectric positioner movement. The slope is the ratio of $\Delta V / \Delta z_c$.

1.1.3.4 Cantilever assembly

In an AFM experiment, the cantilever assembly is mounted on a fluid cell. The assembly, which acts as a force transducer between the tip and the sample, consists two parts: the cantilever and the tip. The cantilever is composed of silicon or silicon nitride. The top surface of the cantilever is often coated with gold to improve reflectivity. The cantilever is normally in rectangular or "V" shaped. The shape, dimensions and the material from which it is made determines the spring constant of the system. The tip, which is located at the end of the cantilever, it is made of the same material as the cantilever. Typically it has a pyramidal shape. In the single molecule force experiments, the tip does not require specific modifications, e.g., a conductive coating or a finely-honed end. The radius of curvature is about 50 nm. The tip provides a point for a molecule to attach itself.

1.1.3.5 Cantilever calibration

To interpret the force data, the spring constant of the cantilever assembly must first be determined. The thermal method is widely used for this purpose. This method is based on the energy equipartition theorem. The cantilever assembly is modeled as a simple harmonic oscillator with one degree of freedom which is oscillated by environmental thermal noise. In this approach, the average potential energy of the cantilever, $\frac{1}{2}k_c < \Delta z_c^2 >$, is equal to the thermal energy, $\frac{1}{2}k_B T$, where, k_c is the spring constant, Δz_c the thermal fluctuation of the cantilever, k_B the Boltzmann constant and T the absolute

temperature. Thus, determination of $< \Delta z_c^2 >$ is required to calibrate of the spring constant. $< \Delta z_c^2 >$ is converted to its corresponding power spectrum by the Fourier transform. The integration over this power density spectrum gives $< \Delta z_c^2 >$. Typically, the error associated with this method is about 20%. On the other hands, it requires no specialized equipment and is easy to perform in a liquid medium. The advantages make it a popular method to determine the spring constant of the cantilever assembly.

1.1.3.6 The vibration isolation system

Since the elongation of a single protein molecule is in the nanometer range, AFM is very sensitive to small movements of either the sample or the cantilever assembly. The vibration isolation system dampens the environmental noise that will reduce the accuracy of the measurement. Consequently, this system is essential for obtaining high quality data. Ideally, for optimal performance, the AFM should be placed under an acoustic proof cover to avoid acoustic noise.

1.1.4 Advantages of polyprotein for AFM studies

It is difficult to acquire the information presented in the force-extension curve by working with a single individually folded domain. The information may be masked by nonspecific interactions between the cantilever tip and the protein layer. The problem of nonspecific interactions is partly overcome by the use of native multidomain protein, like titin. Some of the unfolding events occur at higher extension than the nonspecific

interaction region. However, native multidomain proteins are constituted by heterogeneous domains; moreover, it is difficult to detect the subtle differences between domains. Therefore, it is impossible to identify which peaks correspond to which specific protein domains. This problem has been surmounted by using molecule biological techniques to construct homomeric polyproteins. Polyproteins have a repetitive structure and produce a sawtooth-like force-extension curve. The sawtooth pattern is used as a fingerprint to demonstrate that the single molecule polyproteins is unfolded. This approach also speeds up the data acquisition process because stretching one molecule results multiple unfolding events being analyzed.

1.1.5 A typical force-extension curve

After the polyproteins are adsorbed on the glass coverslip, the protein layer is brought into contact with the cantilever tip. After several approach-retract cycles, a single molecule is picked up by the tip. This molecule is extended by retracting the piezoelectric positioner. When the force exceeds the mechanical stability of one domain in the polyprotein chain, this domain unfolds in an all or none fashion. When the domain unfolds, it becomes extensible. Consequently, the contour length of the polyprotein increases dramatically and the force applying on it falls to a low value quickly. The polyprotein is further stretched until the molecule detaches from the tip or the substrate. The sequential unfolding of protein domains in the polyprotein chain produces a sawtooth pattern in the force-extension curve. The retraction trace serves as a force base line. Each peak except the last one corresponds to the unfolding of a single domain in the polyprotein chain. The last one represents the detachment from either the tip or the

substrate. The mechanical force of each domain is measured from the height of the peaks.

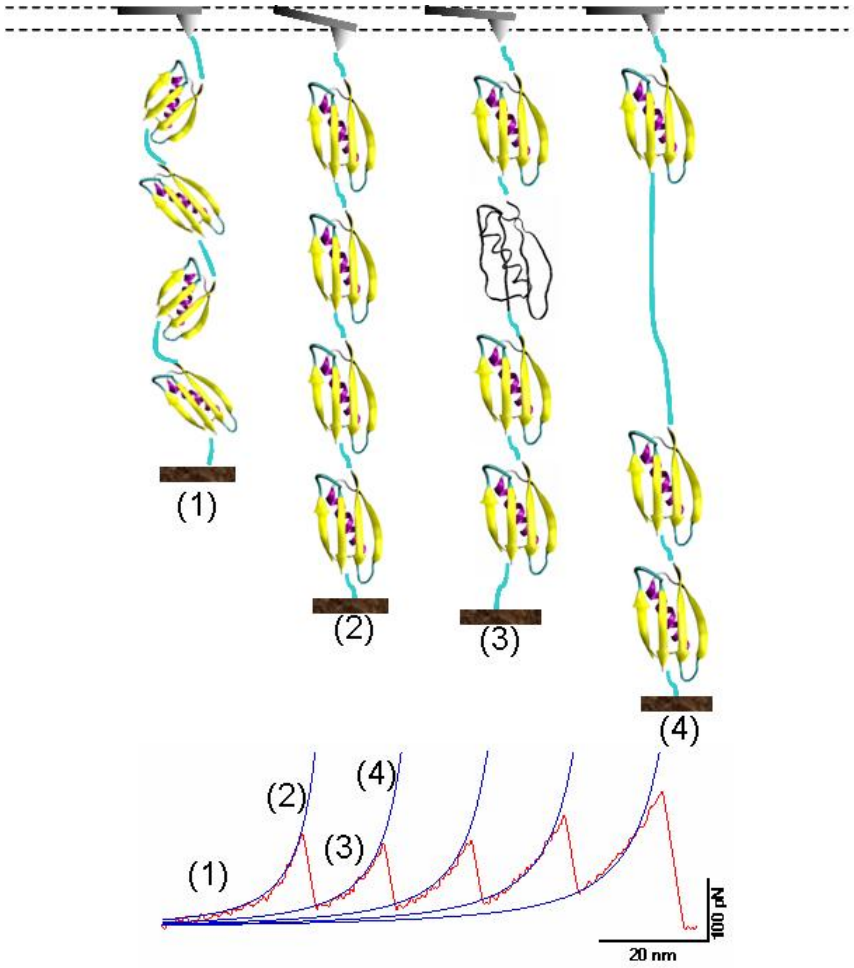

Figure 1.3 Using a single-molecule AFM to measure the elasticity of polyprotein. Top image: the unfolding process of one domain in the polyprotein. Bottom image: the force-extension curve of a polyprotein in a sawtooth pattern fitted by Worm-like Chain model. The last peak corresponds to the detachment from the tip or the positioner. Initially, the polyprotein chain forms a bridge between the piezoelectric positioner and cantilever tip (stage 1). When retracting the piezoelectric positioner, external force is applied to the polyprotein chain. This force is resisted by an entropic restoring force which cause the deflection of the cantilever (stage 2). When one domain is unfolded, the contour length of the polyprotein increases immediately and the cantilever returns to a position that is very close to its initial position (stage 3). By repeating this process, all the domains in the polyprotein will unfold, which produces a characteristic sawtooth pattern curve.

1.1.6 Worm-like chain model and contour length increment

The force-extension curve can be well fitted by the worm-like chain (WLC) model[15-17]. As protein molecules tend to maximize their conformational entropy, when they are extended, a resistance force is generated. This behaviour is called as entropic elasticity. Entropic elasticity can be formally described using the WLC model:

$$F = \frac{k_B T}{p}[\frac{1}{4}(1-\frac{x}{L_c})^{-2} - \frac{1}{4} + \frac{x}{L_c}] \quad (1.3)$$

where k_B and T are the Boltzmann constant and absolute temperature, respectively, p and L_c the persistence length and protein contour length, respectively and x the extension of the protein. Within the WLC model, the resistance force at any given extension of the molecule depends on two parameters: the persistence length p and the contour length L_c. The persistence length defines the flexibility of a protein. The smaller the persistence length, the more the protein resists extension. The contour length is the maximum end-to-end distance. By fitting with WLC model, we are able to measure the contour length increment upon the unfolding of one protein domain. The contour length increment (ΔL_c) is defined as the length of the "force hidden" region of the protein. The contour length increment can be simply calculated by subtracting the length of the folded domain from the fully extended domain. The length of the folded domain is estimated from the crystal structure and the length of the fully extended domain is equal to the number of amino acids within a domain times the average length of one amino acid (~0.36nm). Comparing the theoretically calculated value to the fitted value generated by the WLC model gives an indication of the mechanical structure of the domain.

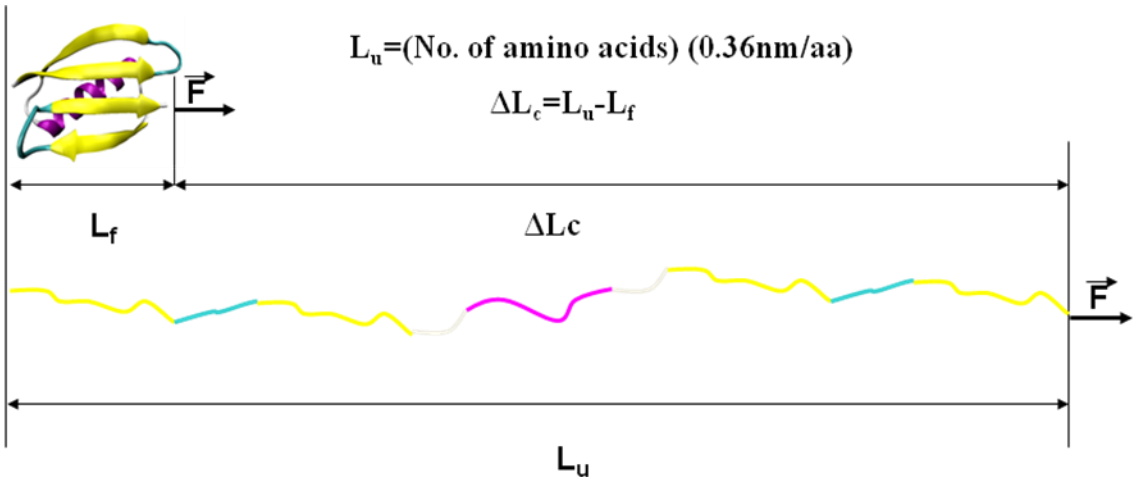

Figure 1.4 Schematic of the relationship of ΔL_c, L_f and L_u. L_u is the contour length of the unfolded protein, which is calculated by multiplying the average length of an amino acid by the number of amino acids in the protein. The contour length increment (ΔL_c) is equal to the difference between the unfolded and folded protein contour length.

1.1.7 The two-state model for protein folding and unfolding

Protein folding/unfolding is often described as a two-state process by conventional transition state theory. The two species, folded and denatured, exchange by crossing a high-energy barrier which is called a transition state. The unfolding and refolding rate constants (k_u and k_f) in this two-state system are given by equations (1.4) and (1.5)

$$k_u = \kappa \frac{k_B T}{h} \exp(-\frac{\Delta G_{TS-N}}{k_B T}) \tag{1.4}$$

$$k_f = \kappa \frac{k_B T}{h} \exp(-\frac{\Delta G_{TS-D}}{k_B T}) \tag{1.5}$$

where κ is the transmission coefficient, k_B the Boltzmann constant, T absolute temperature, h the Planck constant, and ΔG_{TS-N} and ΔG_{TS-D} the activation energies for

unfolding and refolding, respectively.

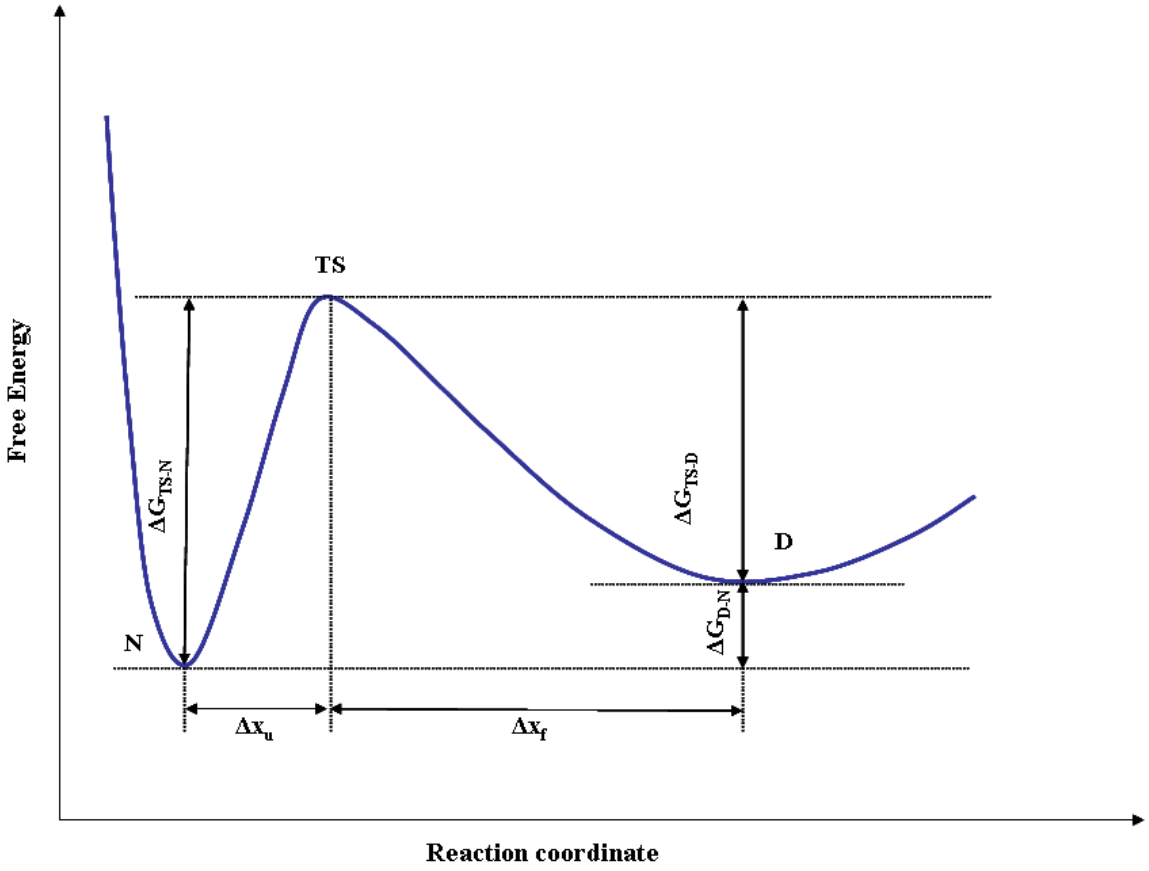

Figure 1.5 Representation of the energy landscape of protein folding and unfolding in the two-state model. N, TS, D represent the native state, the transition state and the denatured state, respectively. Δx_u and Δx_f are the distance from the native state and the denatured state to the transition state along the reaction coordinate, respectively. ΔG_{TS-D} and ΔG_{TS-N} define the kinetic energy barrier for protein folding and unfolding. These two values reflect the folding and unfolding kinetics. ΔG_{D-N} determines the thermodynamic stability of proteins.

1.1.8 The effect of force on the energy landscape

When force is applied, the free energy landscape is tilted. The effect of force on the

intrinsic rate constants of folding and unfolding is described by the Bell-Evans model[18-20].

$$k_u(F) = \kappa \frac{k_B T}{h} \exp(-\frac{\Delta G_{TS-N} - F\Delta x_u}{k_B T}) = k_u^0 \exp \frac{F\Delta x_u}{k_B T} \quad (1.6)$$

$$k_f(F) = \kappa \frac{k_B T}{h} \exp(-\frac{\Delta G_{TS-D} + F\Delta x_f}{k_B T}) = k_f^0 \exp \frac{-F\Delta x_f}{k_B T} \quad (1.7)$$

where, Δx_u is the difference between the native state and the transition state (unfolding distance) and Δx_f the distance between the denatured state and the transition state (folding distance). k_u^0 and k_f^0 are the mechanical unfolding and folding rate constants at zero force, respectively. The energy barrier for unfolding is lowered by $F\Delta x_u$, whereas the energy barrier for refolding is raised by $F\Delta x_f$.

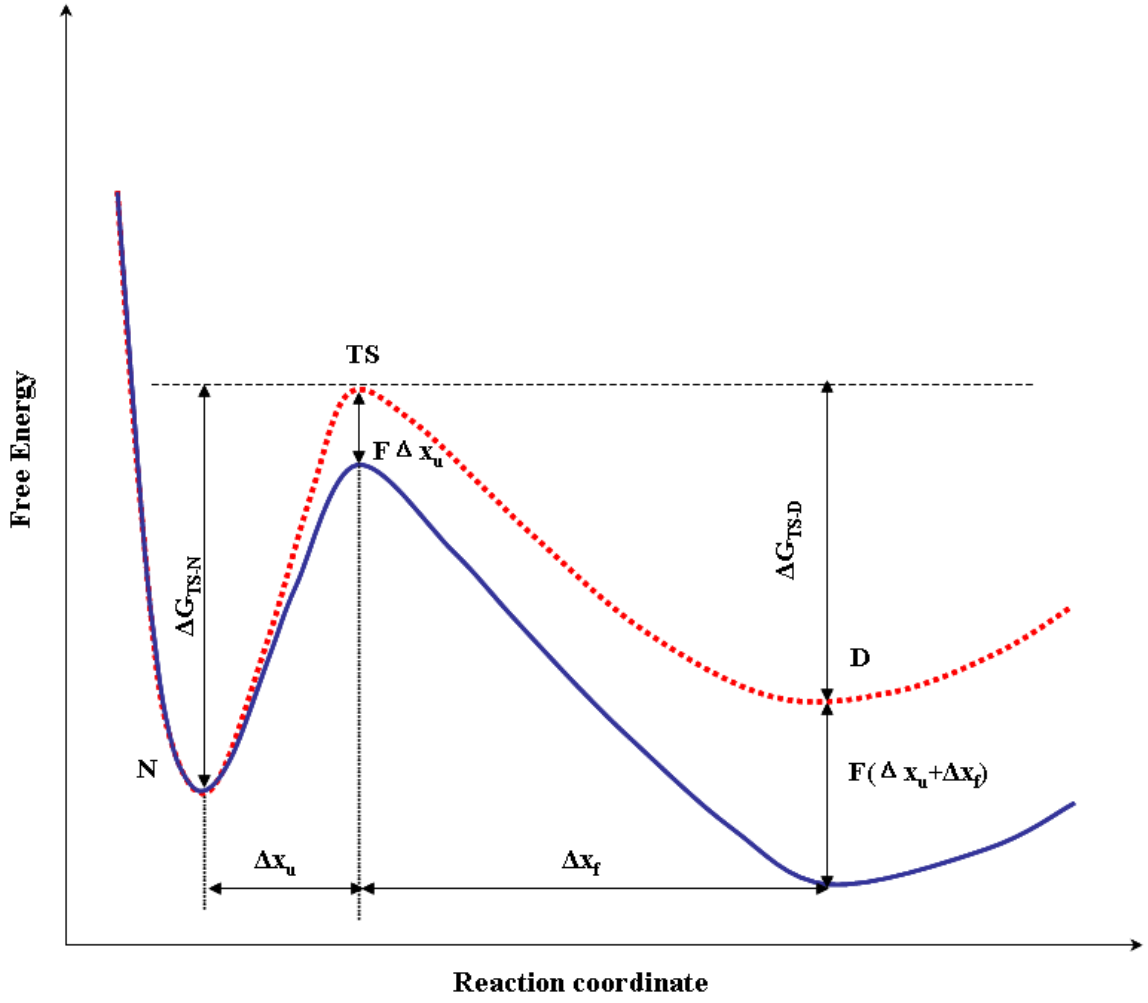

Figure 1.6 The energy landscape of mechanical folding and unfolding in a two state model of protein under force. The blue line indicates the free energy landscape of a protein at zero mechanical force, the red dashed line the energy landscape of protein exposed to a mechanical force. The force destabilizes the native, transition and unfolded states. As a result, the energy barrier for unfolding is lowered by $F\Delta x_u$, whereas the energy barrier for refolding is raised by $F\Delta x_f$.

1.1.9 The non-equilibrium nature of unfolding under force

It is important to note that the mechanical unfolding of a protein is typically a non-equilibrium process. Fig 1.3 (lower graph) indicates hysteresis between the approach and

retract traces, in which mechanical energy is dissipated into heat. In this way, some proteins serve as shock absorbers, dissipating elastic energy to protect proteins and tissue from mechanical damage.

1.1.10 The relationship between unfolding force and pulling speed

Since the mechanical unfolding of proteins is a non-equilibrium process, the unfolding force depends on the loading rate of the force[19]. This was predicated by Evans and verified by experimental work. Protein unfolding is a stochastic event. If the force incensement is linear with the loading rate ($F = a * t$, where a is loading rate, t time), the most probable unfolding force is yielded by:

$$F = \frac{k_B T}{\Delta x_u} \ln \frac{a \Delta x_u}{k_u^0 k_B T} \tag{1.8}$$

where a is the loading rate, Δx_u the unfolding distance, k_u^0 the unfolding rate under zero force, k_B the Boltzmann constant and T absolute temperature. However, in our distance-ramp experiment, force increases in a non-linear fashion with the loading rate. Thus, there is no simple analytical formula to predict the force. Generally, the faster the pulling speed, the higher the average unfolding force will be.

1.1.11 The differences between mechanical stability and thermodynamic stability

The unfolding force of a protein is defined as the mechanical stability. The mechanical

stability of a protein is regulated by the mechanical unfolding energy barrier ΔG_{TS-N} and the unfolding distance Δx_u. A higher mechanical unfolding energy barrier ΔG_{TS-N} and a smaller unfolding distance Δx_u favour a higher unfolding force. ΔG_{TS-N} and Δx_u work in combination. Thus, only a higher mechanical unfolding energy barrier is not necessary to lead to a higher mechanical stability. The thermodynamic stability of a protein depends on the difference between the unfolding state and the native state ΔG_{D-N}. For this reason it is evident that there exists no correlation between the mechanical stability and the thermodynamic stability. Furthermore, the mechanical unfolding pathway differs from the chemical unfolding pathway. Although some proteins have mechanical unfolding rate constants that are similar to their chemical unfolding rate constant, chemical unfolding rate constants cannot be utilized to predict mechanical stability.

1.1.12 Determination of k_u^0 and Δx_u

Since the equation 1.8 cannot be directly applied, Monte Carlo simulation was used to obtain unfolding kinetic information, i.e., the unfolding rate constant at zero force k_u^0 and the unfolding distance Δx_u. These two parameters can be analyzed using Monte Carlo simulation to fit the mechanical unfolding force distribution at certain pulling speeds. The width of the distribution is determined simply by the unfolding distance Δx_u. However, the width may be broadened by experimental errors, such as cantilever drift and thermal noise. Consequently, the results from only fitting the force distribution are not accurate. Normally the simulation is performed for a number of different pulling speeds. Different

pairwise combinations of k_u^0 and Δx_u are tried until the simulation data replicate the experimental unfolding force.

1.2 Design of metal binding sites

Metalloproteins, which play crucial roles in many biological systems[21-24], are termed as proteins that contain one or more metal ions. It is estimated that at least one-third of all proteins have metal cofactors. Design of metal binding sites has attracted considerable attention in protein engineering. Two protein residues binding metal ions represent the simplest metal binding motif. If two metal binding amino acids, like histidine and cysteine, are positioned at appropriate locations, they can form a metal chelating motif, of which the most familiar are bi-histidine motifs. The latter include His-X_3-His in an α-helix, His-X-His in a β-strand, His-X_2-His in a reverse β-strand and two histidines across two strands of an antiparallel β-sheet. Since these motifs are formed by as few as two protein ligands, they are not used to mimic nature metal binding sites. Instead, they are introduced to carry out certain applications, such as protein purification, protein stabilization, regulation of enzymatic activity and mapping protein transition states.

1.2.1 Purification by introducing a bi-histidine site

Sung-sup and co-workers have exploited the His-X_3-His site to purify bovine somatotropin variants in a single step[25]. These two histidines were exposed to a solvent. The metal binding affinity varied from $2*10^{-4}$ to $1.6*10^{-6}$ M^{-1}. They used the surface

accessible bi-histidine site to bind the metal complex Cu(II)IDA. The interaction between the binding site and the metal complex dramatically increased the retention times in a metal affinity chromatography. The affinity depends on the rigidity of solvent accessibility of this site.

However, this method requires a specific secondary structure. A more common method is the His-tag system. Six histidine residues are attached to the N- or C-terminus of protein to facilitate protein purification. This system, which is commercially available, is widely used.

1.2.2 Protein stabilization by bi-histidine-based metal chelation

1.2.2.1 Thermodynamic stability enhancement by a bi-His site

Stabilization of proteins' thermodynamic stability will expand the application of proteins into unusual environments. A traditional strategy to enhance protein thermodynamic stability involves substituting of suitable amino acids. This strategy depends on the structure and amino acid sequences of thermostable proteins. As in some cases this information is not available, a general approach to stabilizing proteins is required. Metal binding to enhance protein thermodynamic stability can be divided into two classes. One approach is achieved by adding kinetically labile metals such as Cu^{2+}, Ni^{2+} and Zn^{2+}. These metal ions preferentially bind to the native rather than the denatured proteins. The other one involves adding substitution-inert metal ions, like Ru^{2+} and Co^{3+}. This metal mediated crosslink is similar to a disulfide bridge.

Figure 1.7 shows a thermodynamic cycle for a two state protein folding/unfolding transition. It explains the mechanism of stabilization by kinetically labile metal ions. When the secondary structure of folded proteins feature the kind of geometry that matches the stereochemical requirements of metal ions, kinetically labile metal ions can bind preferentially and stabilize the folded proteins. As illustrated in Figure 1.7, the difference in the free energy of proteins unfolding in the presence and absence of metal ions is equal to the difference in energy between the unfolded and native state. The Arnold group has successful exploited this mechanism to stabilize a small protein, cytochrome c[26]. The group constructed two variants of cytochrome c. Cytochrome c has a histidine at position 39. They introduced a new histidine to position 58. These two histidines are located across an antiparallel β-sheet ($H_{39}H_{58}$). The other variant had a His-X_3-His motif in the N-terminal α-helix. The two histidines are introduced at amino acid positions 4 and 8 (H_4H_8). Addition of Cu^{2+} ions enhanced the stability of $H_{39}H_{58}$ by 2.7 $kCalmol^{-1}$ and H_4H_8 by 1.2 $kCalmol^{-1}$.

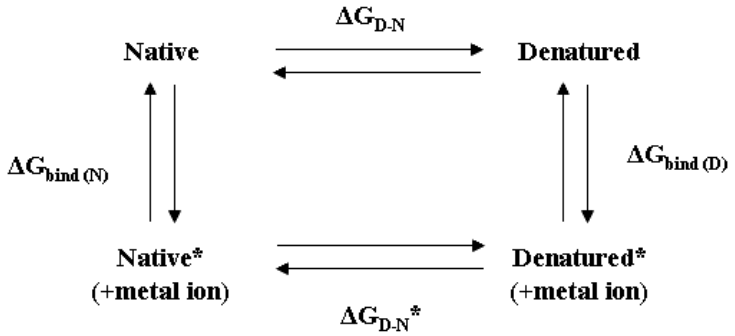

Figure 1.7 Thermodynamic cycle of metal binding to the native and denatured state. The asterisks represent protein in the metal binding state. $\Delta\Delta G_{D-N}$ is defined as $\Delta G_{D-N}{}^{*} - \Delta G_{D-N}$. $\Delta\Delta G_{bind}$ is $\Delta G_{bind(D)} - \Delta G_{bind(N)}$. The cycle indicates that $\Delta\Delta G_{D-N} = \Delta\Delta G_{bind}$. Thus, the preferential binding of metal ions to the native state stabilizes the thermostability of proteins.

Substitution-inert metal ions and kinetically labile metals differ in that ther former remain bound when a protein unfolds. This metal mediated crosslink resembles a disulfide bridge. Andreas et al studied the same two variants of cytochrome c[27]. A Ru(II) complex stabilized the variant $H_{39}H_{58}$ by 5.5 kCalmol^{-1}. However, the H_4H_8 cytochrome c was not stabilized by cross linking with the Ru(II) complex. The stabilization mechanism was thought to be entropic destabilization of the unfolded state, so stabilization relied on the size of the loop created by the metal mediated cross link. The loop of the H_4H_8 variant was only 4 amino acids long, so the conformational entropy of the unfolded protein would not be dramatically destabilized.

1.2.2.2 Mechanical stability enhancement by a bi-His site

As discussed above, mechanical stability is defined as the force required to unfold a protein. This differs from thermodynamic stability, which is the free energy difference between the folded and unfolded state. Mechanical stability is a function of the mechanical unfolding energy barrier and unfolding distance. The mechanical unfolding energy barrier is the energy difference between the native and mechanical transition state. If assuming the unfolding distance does not change, a figure similar to figure 1.7 can be drawn. As figure 1.8 shows, $\Delta\Delta G_{TS-N} = \Delta G_{bind(TS)} - \Delta G_{bind(N)}$. If metal ions preferentially bind to the native state rather than the transition state, the mechanical unfolding energy barrier increases. As a result, the mechanical stability will be enhanced. Cao et al. demonstrated this mechanism by engineering five bi-histidine GB1 mutants[28]. These variants can be classified into three types, two histidines located across antiparallel β-sheet (H_4H_{51}, H_6H_{53} and H_8H_{55}), a His-X_3-His motif in the α-helix ($H_{32}H_{36}$) and a His-X-

His site in the first β-strand (H_4H_6). The thermodynamic stability of all five variants was increased by adding Ni^{2+} ions. But only bi-histidine chelating sites located across antiparallel β-sheet enhanced the mechanical stability after binding with metal ions. For the other two motifs, no mechanical stability enhancement occurred because H_4H_6 and $H_{32}H_{36}$ were well formed at the transition state. Metal binding stabilized the native state to the same degree as the transition state. The mechanical unfolding energy barrier underwent no change, and mechanical stability enhancement was not achieved.

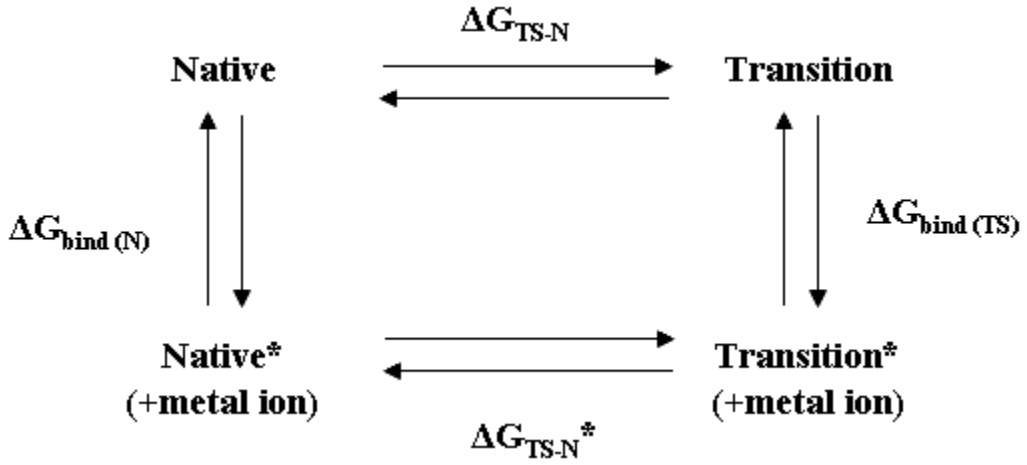

Figure 1.8 Thermodynamic cycle of metal binding to the native and mechanical transition state. The asterisks represent protein in the metal binding state. $\Delta\Delta G_{TS-N}$ is defined as $\Delta G_{TS-N}{}^{*} - \Delta G_{TS-N}$ and $\Delta\Delta G_{bind}$ as $\Delta G_{bind(TS)} - \Delta G_{bind(N)}$. Thus, $\Delta\Delta G_{TS-N} = \Delta\Delta G_{bind}$. The mechanical stability of proteins can be enhanced by the preferential binding of metal ions to the native state rather than the transition state.

1.2.3 Regulation of enzymatic activity

Trypsin is an enzyme used to catalyze the hydrolysis of proteins. Craik et al. engineered a histidine residue to form a bi-histidine chelating site with an exciting histidine in the

trypsin[29]. This exciting histidine is located in the enzyme active site. The mutant trypsin retained its enzymatic activity. Addition of metal ions dramatically inhibited this activity. This was because the histidine residue at the active site rotated out to participate in metal binding with the introduced histidine. This inhibition was fully reversed upon addition of EDTA. Thus, this metal binding site acted as a switch to regulate enzymatic activity.

1.2.4 Probing protein unfolding pathway

The Sosnick group developed a Ψ-analysis method to analyze protein folding transition states[30-32]. This method uses bi-His metal chelation sites. The group engineered one bi-histidine metal binding site into proteins, after which the site was used to investigate the transition state. The advantage is that one pair of bi-histidine site can probe a specific region, thus overcoming the ambiguity in Φ -analysis. Metal ions continuously stabilize the interaction between the two histidine residues by increasing metal ion concentration. Thus, the Ψ -value is defined as:

$$\Psi_U = \delta(\Delta\Delta G_{TS-N}) / \delta(\Delta\Delta G_{D-N}) \tag{1.9}$$

A Ψ -value of 0 indicates that this bi-His site is native-like in the transition state because the stabilization of the metal ion binding must be equivalent to the stabilization achieved in the native state. A Ψ -value of 1 indicates this site is not formed in the transition state. A fraction Ψ -value can be interpreted by heterogeneity in the transition state or transition state distortion. In the heterogeneity model, the value observed is indicative of the fraction of the ensemble that is native formed in the transition state. In the distortion model, the fraction value is derived from the non-native binding energy in the transition

state.

1.3 Objectives

In this thesis, we mainly use single molecule AFM to study the mechanical properties of a small protein GB1, the B1 IgG binding domain of protein G from Streptococcus[33]. This study has two objectives: to probe the mechanical transition state of GB1 by mechanical Ψ-value analysis and to enhance the mechanical stability of a GB1 mutant by binding it with different metal ions.

1.3.1 Probing the mechanical transition state of GB1 by mechanical Ψ-value analysis

Understanding protein folding/unfolding mechanisms is one of the central goals in the life science[34-36]. The transition state is the highest point on the energy landscape. Characterizing the structure and energy levels of the transition state is critical to understanding the folding/unfolding mechanism. However, due to its high free energy, the transition state cannot be trapped and detected by the usual structural methods such as NMR or X-ray crystallography.

In Chapter 3, we adopted the chemical Ψ-value analysis to probe the mechanical unfolding transition state of the protein of interest. The mechanical Ψ-value is defined as:

$$\psi_U^{M2+} = \Delta\Delta G_{TS-N} / \Delta\Delta G_{D-N} \quad (1.10)$$

It is worthy note that in chemical Ψ-value analysis, the Ψ-value is defined as the

infinitesimal change in activation free energy compared to the infinitesimal change in thermodynamic stability as described in equation 1.9. However, metal-bound and metal-free forms of bi-His mutants have distinct mechanical stabilities[28, 37]. Hence, the mechanical Ψ_U value reduces to ψ_U^{M2+}. Assuming $\Delta\Delta G_{D-N}$ is the difference of ΔG_{D-N} of bi-His mutant with and without divalent metal ions as calculated from chemical denaturation. $\Delta\Delta G_{TS-N}$ is the difference energy barrier between the transition state and the native state in the absence and presence of metal ions. It is calculated by equation 1.11:

$$\Delta\Delta G_{TS-N} = -RT\ln[k_u^0(metal-bound)/k_u^0(metal-free)] \quad (1.11)$$

As we know from 1.2.2.2, $\Delta\Delta G_{TS-N}$ is equal to the difference in binding energy of the metal ion to the native state and the mechanical unfolding transition state $\Delta G_{bind(TS)} - \Delta G_{bind(N)}$. As described in figure 1.8, if the metal chelation site is as formed in the mechanical unfolding transition state as in the native state, the metal ions will stabilize the transition state the same degree as the native state, $\Delta G_{bind(TS)} = \Delta G_{bind(N)}$. In this case, $\Delta\Delta G_{TS-N} = 0$ and $\psi_U^{M2+} = 0$. If the metal chelation site is completely unstructured, $\Delta\Delta G_{TS-N} = \Delta\Delta G_{U-N}$ and $\psi_U^{M2+} = 1$. If the metal chelation site is partially disrupted, $0 < \psi_U^{M2+} < 1$.

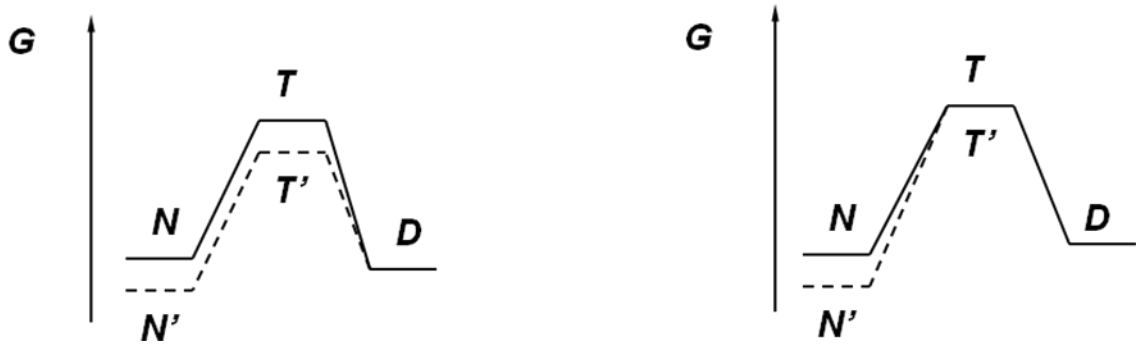

Figure 1.9 Energy diagram for the two extremes of ψ_U^{M2+} for mechanical unfolding of proteins. If the metal chelation site is as formed in the mechanical unfolding transition state as in the native state, $\Delta\Delta G_{TS-N} = 0$ and $\psi_U^{M2+} = 0$; if the metal chelation site is completely disrupted in the mechanical unfolding transition state, $\Delta\Delta G_{TS-N} = \Delta\Delta G_{D-N}$ and $\psi_U^{M2+} = 1$

Our results showed that the contacts between the force-bearing strands 1 and 4 are largely disrupted at the transition state, while the first β-hairpin and α-helix are largely intact. The second hairpin is partially disrupted. These results are in close agreement with MD simulations for which that provide a benchmark.

1.3.2 Enhancing the mechanical stability of a GB1 mutant by chelating different metal ions

Elastomeric proteins are subject to stretching forces under their natural environments and serve as the basic building blocks in a wide variety of biological tissues and biomaterials of superb mechanical properties[38-46]. The mechanical stability of constituting domains in elastomeric proteins determines the working of elastomeric proteins. Thus, tuning the mechanical stability of proteins in a rational fashion is a challenge for protein engineers.

It tests our understanding of the molecular determinants of mechanical stability. Several strategies have been developed successfully to rationally regulate the mechanical stability of proteins, including rational control of the unfolding pathway by disulfide bond formation[47], improving hydrophobic packing[48], reconstruction of the force-bearing region of proteins[49, 50], ligand binding[51-54], and engineered metal chelation[28, 55].

In chapter 4, we investigated the mechanical stability of G6-53 using four different divalent metal ions. We showed all these four metal ions enhance the mechanical stability of G6-53 by different degrees. As this process is completely reversible, proteins can be used as a switch. Moreover, the resultant unfolding force difference between Co^{2+} and Zn^{2+} or Zn^{2+} and Cu^{2+} is ~ 20 pN. Thus, various metal ions can be used to fine tune the mechanical stability of proteins

Chapter 2 Materials and methods

2.1 Engineering polyprotein genes

The plasimid encoding wild type GB1 was a generous gift from Prof. David Baker of the University of Washington, Seattle. All the bi-His mutants were constructed using the mega primer method and confirmed by direct DNA sequencing. A well-estabilished multiple-cloning strategy was adopted to engineer the plasmid of octamer genes. The DNA monomer is flanked by a 5' BamHI and 3' BglII, KpnI restriction sites. The sticky ends digested by enzymes BamHI and BglII are identical. As a result, these two sticky ends can be perfectly ligated. It is of note that the new sequence cannot be digested by either the BamHI or BglII enzyme. Figure 2.1 describes a basic multiple-cloning strategy for construction a polyprotein gene. First, the plasmid containing the DNA monomer is digested by BamHI and KpnI to produce the insert; this plasmid is also digested by BglII and KpnI to yield the vector. Second, the vector and insert are ligated into a circular plasmid by the T4 ligase. Third, the resulting dimmer plasmids are transformed into XL1/Blue competence cells. Fourth, the DNA plasmids are purified from the E coli cells by mini-prep. Lastly, the size of the dimmer is confirmed by agarose gel electrophoresis. By repeating these steps, we can build a tetramer and octamer. Typically, we use pUC19 during multiple cloning steps and transfer the final constructs to the expression vector pQE80L. The pQE80L vector contains a T5 promoter and a $(His)_6$ tag at the N-terminal to facilitate protein purification.

Table 2.1BamHI BglII and KpnI restriction sites

	BamHI	BglII	KpnI
Cut site	5’ GGATCC 3’ 3’ CCTAGG 5’	5’ AGATCT 3’ 3’ TCTAGA 5’	5’ GGTACC 3’ 3’ CCATGG 5’
Overhang	5’ G GATCC 3’ 3’ CCTAG G 5’	5’ A GATCT 3’ 3’ TCTAG A 5’	5’ GGTAC C 3’ 3’ C CATGG 5’

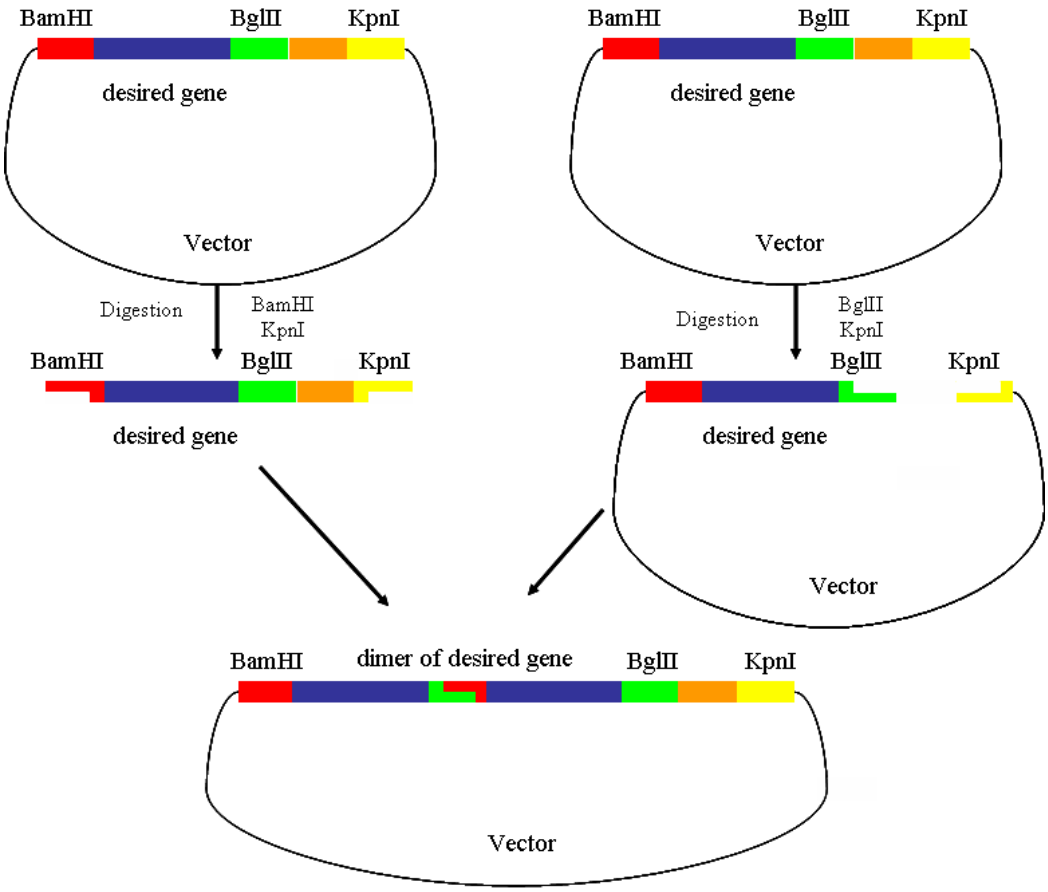

Figure 2.1 General procedures for engineering the polyprotein gene. Digestion with restriction enzymes produces the desired insert and vector. The vector and insert are ligased to make a dimmer. The gene of the tetramer and the octarmer can be constructed sequentially by repeating this procedure.

2.2 Polyprotein expression and purification

Polyprotein was expressed in an E coli system. The plasmid carrying the target polyprotein gene was transformed into DH5α competent cells and grown overnight at 37 ℃ on an agar plate. The agar plate contained a 2.5% Luria-Bertani broth (LB), 2% agar and 10mg/cm3 ampicillin. Next one colony was chosen to grow in 5mL 2.5% LB containing 10 mg/L ampicillin over night at 37 ℃ and 225 rpm. The resulting culture was

inoculated into 300 L of a LB medium (1/100 dilution) containing 10 mg/L ampicillin and grew at 37 ℃ and 225 rpm until the optical density (OD) was between 0.6-1. Protein expression was induced by adding Isopropyl-1-β-D-thiogalactoside (IPTG) with a final concentration of 1 mM. The cell culture was further incubated for 3-4 hours at 37 ℃ and 225 rpm. The cells were harvested by centrifugation at 4000rpm for 15min. The supernatant was discarded and the cells were lysised by 1mg/mL lysozyme for 30 min on ice. The DNAs and RNAs were digested by 0.005mg/mL Dnase I and Rnase A. Following digestion, the mixture was centrifuged at 12000rpm for 60min and the soluble fraction was passed through Co^{2+} affinity chromatography. The column was washed with a 200 mL washing buffer (10mM phosphate buffer with 300mM NaCl and 7mM imidazole) and eluted with a 3ml elution buffer (10 mM phosphate buffer saline (PBS) with 250mM imidazole). Residual Co^{2+} ions were removed by adding 20mM EDTA to the elution fraction, and the EDTA and imidazole were removed by dialysis against the Tris-HCl buffer (10 mM, pH 7.4, containing 100 mM NaCl).

2.3 Chemical denaturation

Chemical denaturation experiments were carried out using a Cary Eclipse Fluorescence Spectrophotometer. The unfolding process was probed by exciting Tryptophan of all bi-His mutants at 280 nm and monitoring the emission spectra at 360 nm. Figure 2.2 shows the representative G8-55 fluorescence intensity as a function of molar GdmCl concentration. This graph can be broken into three sections. At low GdmCl concentrations, the curve is flat. This section is called the native baseline (y_n). As the

GdmCl concentration increases, the slope turns steep. In this section, labeled as transition region, the native and denatured forms coexist. When the GdmCl concentration increases further, the curve again flattens. It is called the denatured baseline (y_d).

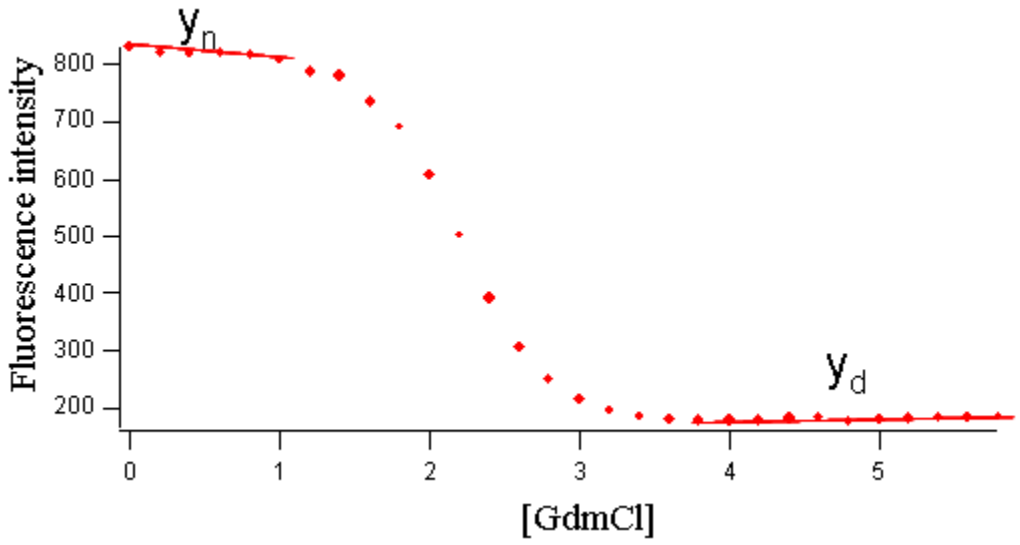

Figure 2.2 GdmCl induced unfolding of G8-55 monitored by fluorescence spectrophotometer. The native and denatured baseline regions are separated by a transition region.

We assume all the mutants are folding/unfolding in a simple two-state model:

$$N \rightleftharpoons D \tag{2.1}$$

$$K_{eq} = \frac{[D]}{[N]} \tag{2.2}$$

$$\Delta G^0 = -RT \ln K_{eq} \tag{2.3}$$

where K_{eq} is the equilibrium constant, $[D]$ and $[N]$ the protein concentrations in the native and denatured state at equilibrium, respectively, R the gas constant, T the absolute temperature and ΔG^0 the free energy of protein folding at each denaturant concentration.

According to equation 2.4, the fluorescence intensity can be converted to the unfolding fraction, yielding the relationship expressed in the graph below.

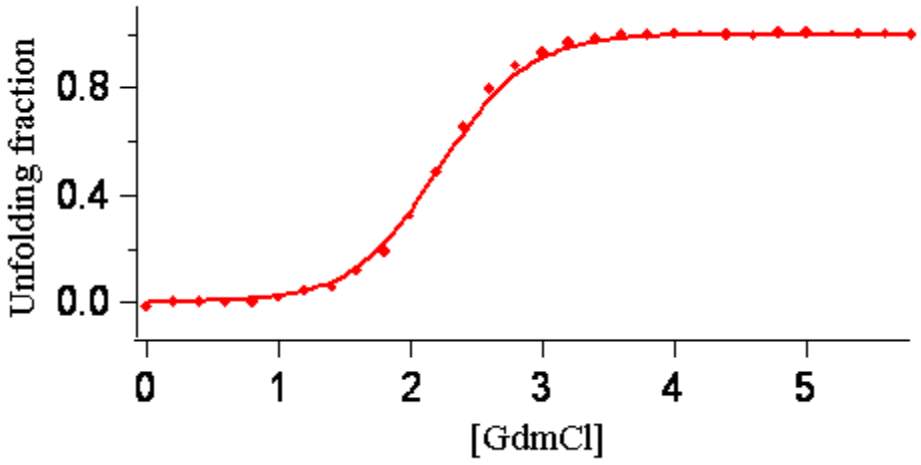

Figure 2.3 Unfolding fraction of G8-55 as a function of [GdmCl]. The curve is fitted by equation 2.7

$$F_d = \frac{[D]}{[D]+[N]} = \frac{y_n - y_{obs}}{y_n - y_d} = \frac{K_{eq}}{1+K_{eq}} \tag{2.4}$$

where, y_n and y_d are the native and denatured baselines, respectively and y_{obs} the fluorescence intensity at a specific GdmCl concentration.

The folding free energy ΔG^0 varies linearly with the denaturant concentration:

$$\Delta G^0 = \Delta G^0_{water} - m[D] \tag{2.5}$$

where ΔG^0_{water} is the free energy of unfolding in the absence of a denaturant and m the slope of the transition region. Substituting equation 2.5 for 2.3, yields:

$$K_{eq} = \exp((m*[D] - \Delta G^0_{water})/RT) \tag{2.6}$$

Thus,

$$F_d = \frac{\exp((m*[D] - \Delta G^0_{water})/RT)}{1+\exp((m*[D] - \Delta G^0_{water})/RT)} \quad (2.7)$$

The data were fitted to equation 2.7 to measure the thermodynamic stability of a given protein.

2.4 Single-molecule AFM

Single molecule AFM experiments were carried out in a custom-built atomic force microscopy as described above[37, 56]. Two different buffers were used in the experiments: Tris-HCl (10mM, pH 7.4, containing 100 mM NaCl) and Tris-HCl plus one of four metal ions, Ni^{2+}, Co^{2+}, Zn^{2+} and Cu^{2+}. Prior to each experiment, the cantilever was calibrated by means of equipartition theorem to determine the spring constant. In a typical experiment, a polyprotein solution was deposited onto a clean coverslip covered with a 50 ul Tris-HCl buffer. For metal ions binding experiments, 14.3 mM metal ions were added to the mixture of protein and Tris-HCl. The AFM experiments were performed after 10-20 mins to allow the mixture to be equilibrated. The pulling speed for all unfolding experiments is 400nm/s, unless specified otherwise.

2.5 Monte Carlo simulation

Since there is no simple numerical solution to calculate the unfolding rate constant at zero force k_u^0 and unfolding distance Δx_u, Monte Carlo simulation was used to estimate these two parameters. In this simulation, the polyprotein is extended by AFM at a constant speed v_c over a discrete time interval of Δt. As a result, the extension of polyprotein

is $x = v_c * t$. The force generated can be calculated from the WLC model. Polyprotein unfolding probability is given by $P_U = N_f k_u \Delta t$, where N_f the number of folded domains, k_u is the unfolding rate constant and Δt the time interval. k_u is calculated from equation 1.6: $k_u(F) = k_u^0 \exp \frac{F \Delta x_u}{k_B T}$. Next P_U is compared with a random number, If P_U is greater than the random number, we assume the protein is unfolded and the force at time t is the unfolding force.

The simulation results are used to fit the experimental data until they reflect the unfolding force obtained experimentally by adjusting the combinations of k_u^0 and Δx_u .

Chapter 3 Mapping the structure of the mechanical unfolding transition state of an elastomeric protein domain GB1 by engineering bi-histidine metal chelation sites

3.1 Results

3.1.1 Engineered bi-His GB1 variants

We constructed nine bi-His mutants. These mutants can be classified into three categories differentiated by the location of bi-histidine substitution in GB1: (1) mutants across the β-strands 1 and 4, which probe the structure of the force-bearing region (G4-51, G6-53 and G8-55); (2) mutants across β-strands 1 and 2 or 3 and 4, which probe the structure of the two β hairpins (β hairpin 1 and β hairpin 2) in the mechanical unfolding transition state (G4-17, G6-15, G44-53 and G42-55); (3) mutants at the α-helix, which probe the structure of the α-helix in the transition state (G32-36 and G24-28).

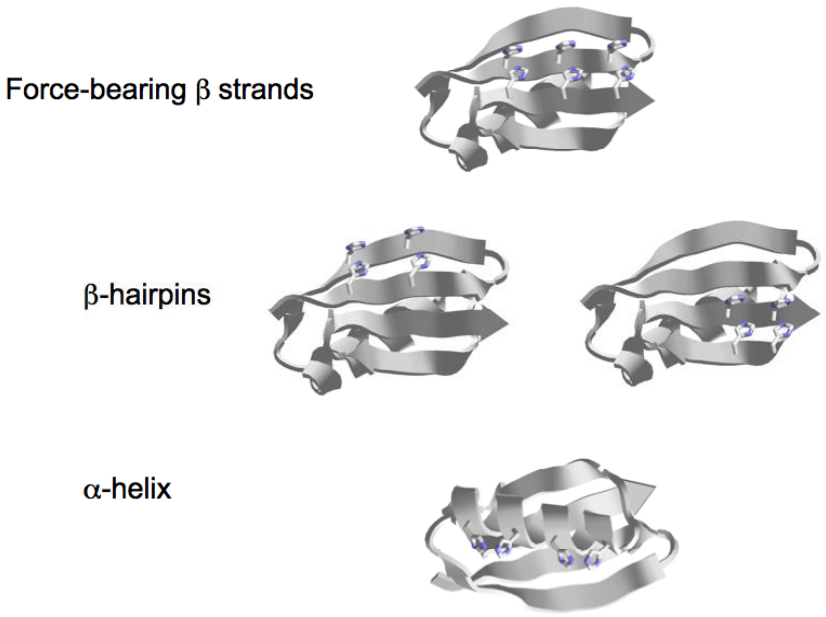

Figure 3.1 Bi-histidine mutants of GB1 designed to probe different regions of GB1 in its mechanical unfolding transition state. Mutants G5-51, G6-53 and G8-55 are designed to probe the structure of the force-bearing strands in the transition state, G4-17, G6-15, G44-53 and G42-55 are designed to probe the structure of the two β-hairpins in the transition state, and mutants G24-28 and G32-36 are designed to probe the structure of the α -helix in the transition state.

3.1.2 Equilibrium binding of Ni^{2+} to GB1 bi-His mutants

We first carried out chemical denaturation experiments to quantify the effect of metal binding (Ni^{2+}) on the thermodynamic stability of GB1 bi-His mutants in the presence of a saturating Ni^{2+} concentration. Representative chemical denaturation curves are shown in Figure 3.2; equilibrium free energies in the absence and presence of Ni^{2+} are shown in Table 3.1. It is clear that the thermodynamic stability of all bi-His mutants, except G6-15 and G44-53, increase upon their binding with Ni^{2+}, as evidenced by the increasing $[GdmCl]_{0.5}$ of the bi-His mutants in the presence of Ni^{2+} compared with the $[GdmCl]_{0.5}$ in

the absence of Ni^{2+}. $[GdmCl]_{0.5}$ is the concentration of GdmCl at which 50% of the proteins are unfolded. These results suggest that in their native state these bi-His mutants can bind with Ni^{2+} with a high binding affinity. Mutants G6-15 and G44-53 are two exceptions. G43-55 does not show obvious binding to Ni^{2+}, suggesting that the geometry/conformation of bi-histidine 42 and 55 does not confer a significant metal binding affinity. Thus G44-53 is not a good candidate for φ_U^{M2+}-value analysis. It is interesting to note that mutant G6-15 shows an abnormal behavior upon binding with Ni^{2+}: This binding leads to a reduction in the thermodynamic stability of G6-15, instead of the expected stabilization effect upon binding of Ni^{2+}. This abnormal behavior suggests that the binding of Ni^{2+}destabilized the native state of G6-15. Inspecting the structure and sequence of GB1, we notice that the charged Lys4 is adjacent to the bi-His-Ni^{2+} site of the mutant G6-15. It is possible that repulsive electrostatic interactions between Lys4 and Ni^{2+} may be responsible for the destabilization effect. Although the effect of Ni^{2+} binding for G6-15 is destabilizing, its thermodynamic and mechanical effect can, nonetheless, be used to evaluate the structure of the mechanical unfolding transition state.

It is important to note that for bi-His mutants the equilibrium free energy change $\Delta\Delta G_{U-N}$ upon binding with Ni^{2+} reported in Table 3.1 is at 14.3 mM Ni^{2+}. Since $\Delta\Delta G_{U-N}$ is dependent upon the concentration of Ni^{2+}, $\Delta\Delta G_{U-N}$ should also depend on the concentration of Ni^{2+}. Since 14.3 mM Ni^{2+} is close to the saturating concentration, $\Delta\Delta G_{U-N}$ at 14.3 mM Ni^{2+} is close to $\Delta\Delta G_{U-N}$ at the saturating concentration of Ni^{2+}. For the sake of simplicity, here we use $\Delta\Delta G_{U-N}$ at 14.3 mM Ni^{2+}as the thermodynamic

stability difference caused by the binding with Ni^{2+}.

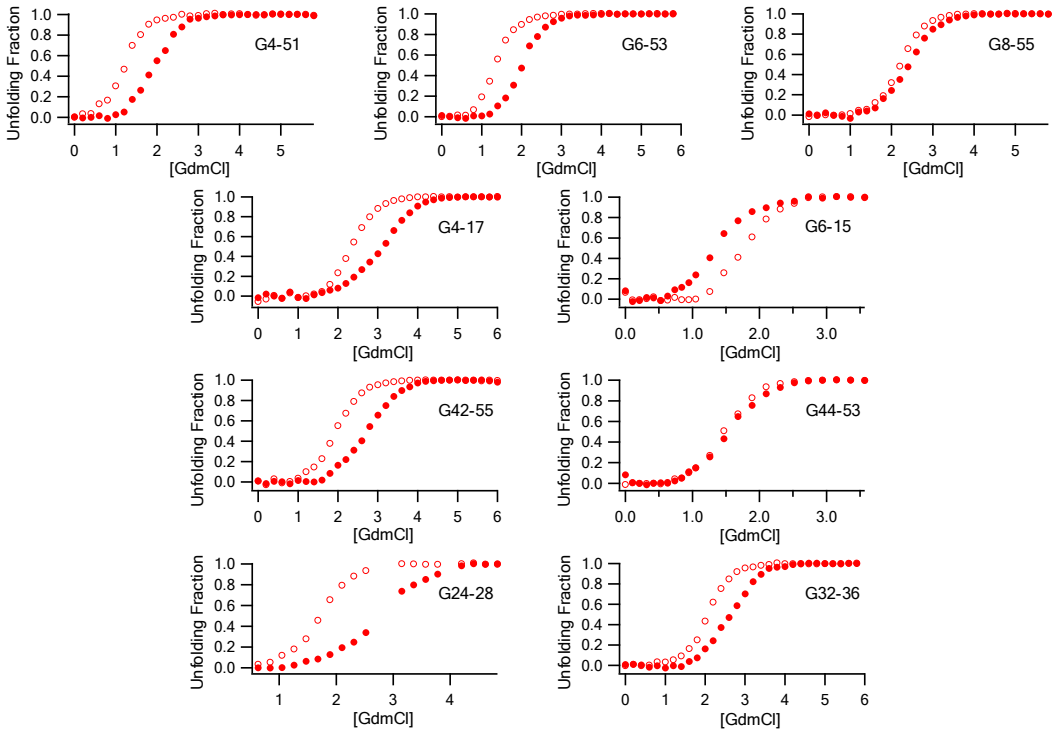

Figure 3.2 The binding of Ni^{2+} increases the thermodynamic stability of GB1 bi-His mutants except G6-15 and G44-53. All the figures are representative equilibrium chemical denaturation curves of bi-His mutants in different regions of GB1. Red open symbols correspond to chemical denaturation curves in the absence of Ni^{2+}, while the filled symbols correspond to chemical denaturation curves in the presence of 14.3 mM Ni^{2+}.

3.1.3 The effect of Ni^{2+} binding on the mechanical unfolding of GB1 bi-His mutants

We used single molecule force spectroscopy techniques to investigate the effect on the mechanical stability of GB1 bi-His mutants following binding with Ni^{2+}. Stretching (bi-His-mutant)$_8$ polyproteins resulted in force-extension curves featuring a characteristic

sawtooth pattern, where individual sawtooth peaks correspond to the mechanical unfolding of the individual domains in the polyprotein chain. Figure 3.3 shows typical force-extension curves for all bi-His mutants in the absence and presence of 14.3 mM Ni^{2+}. The unfolding force histograms for each mutant in the absence and presence of 14.3 mM Ni^{2+} are shown in Figure 3.4. It is clear that the unfolding forces of different mutants change differently upon binding with Ni^{2+}. The unfolding forces of some bi-His mutants can increase as much as 100%, for example, G6-53, whereas for others, there is no change at all, for example, G4-17, suggesting that binding with Ni^{2+} has different effects on the mechanical unfolding energy barrier for different bi-His mutants.

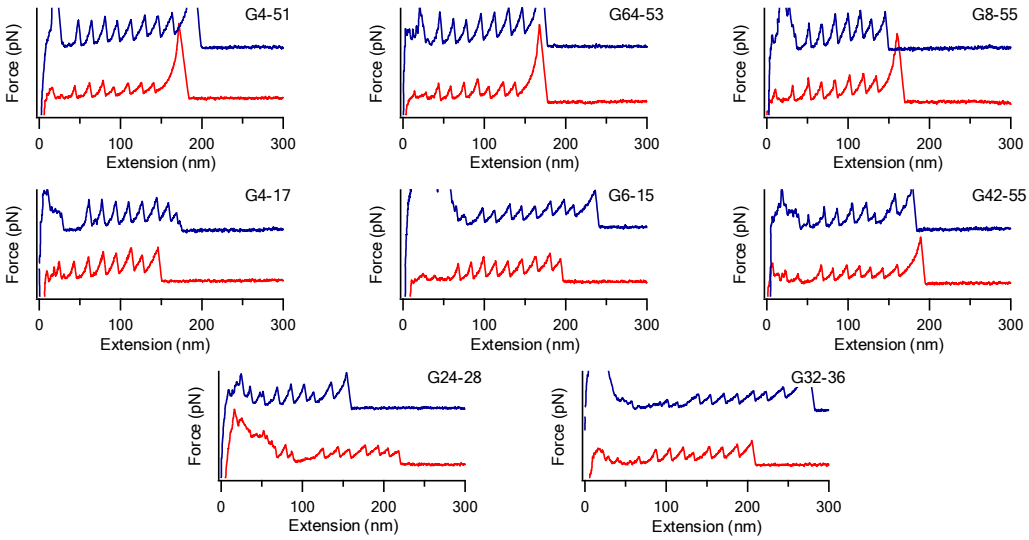

Figure 3.3 Typical force–extension curves for different bi-His mutants in the absence (red) and presence (blue) of 14.3 mM Ni^{2+}

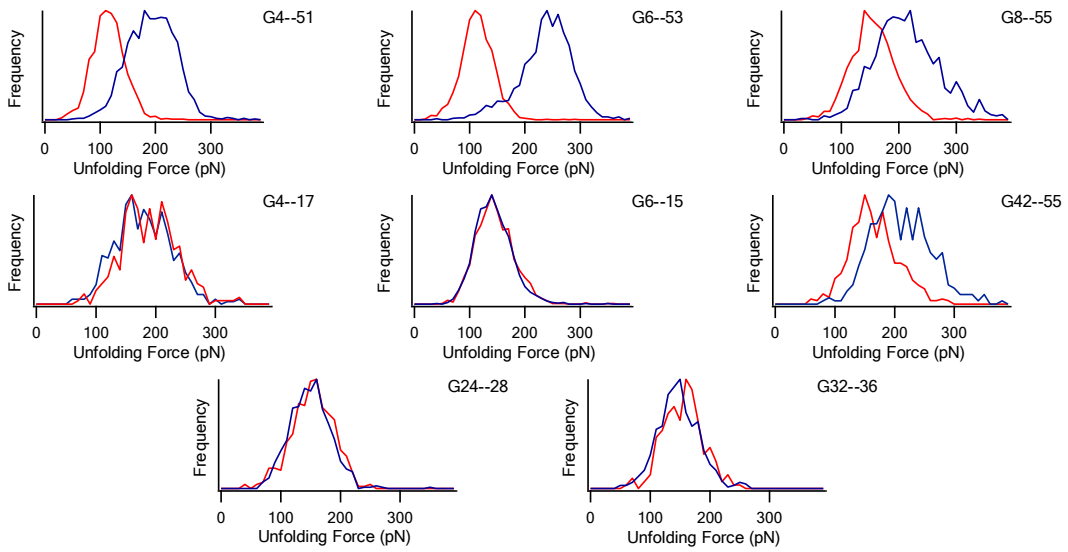

Figure 3.4 Unfolding force histograms for different bi-His mutants in the absence (red) and presence (blue) of 14.3 mM Ni^{2+}. The mechanical stabilities of G4-51, G6-53, G8-55 and G42-55 are enhanced by binding with Ni^{2+} ions. There is no obvious force increment for G4-17, G6-15, G24-28 and G32-36 mutants.

To quantify the change in the mechanical unfolding energy barrier upon Ni^{2+} binding, we carried out force-extension experiments at different pulling speeds. The representative pulling speed dependences of the unfolding forces are shown in Fig 3.5. Using well-established Monte Carlo simulation procedures[4, 41, 57], we fitted the unfolding force distribution and pulling speed dependence of the unfolding force simultaneously to estimate the spontaneous unfolding rate constant k_u^0 at zero force as well as the distance between the native state and the mechanical unfolding transition state Δx_u. Based on k_u^0, we then calculated the change in the mechanical unfolding free energy $\Delta\Delta G_{TS-N}$ using the following relationship:

$$\Delta\Delta G_{TS-N} = -RT \ln[k_u^0(metal-bound)/k_u^0(metal-free)]$$

The results are summarized in Table 3.1.

Having measured the equilibrium free energy change ($\Delta\Delta G_{D-N}$) as well as the mechanical unfolding free energy change ($\Delta\Delta G_{TS-N}$), we can now determine the mechanical φ_U^{M2+} value for the mechanical unfolding of GB1 and map the mechanical unfolding transition state. It is evident that the three structural regions of GB1 show different mechanical φ_U^{M2+} values (Figure 3.5 and Table 3.1).

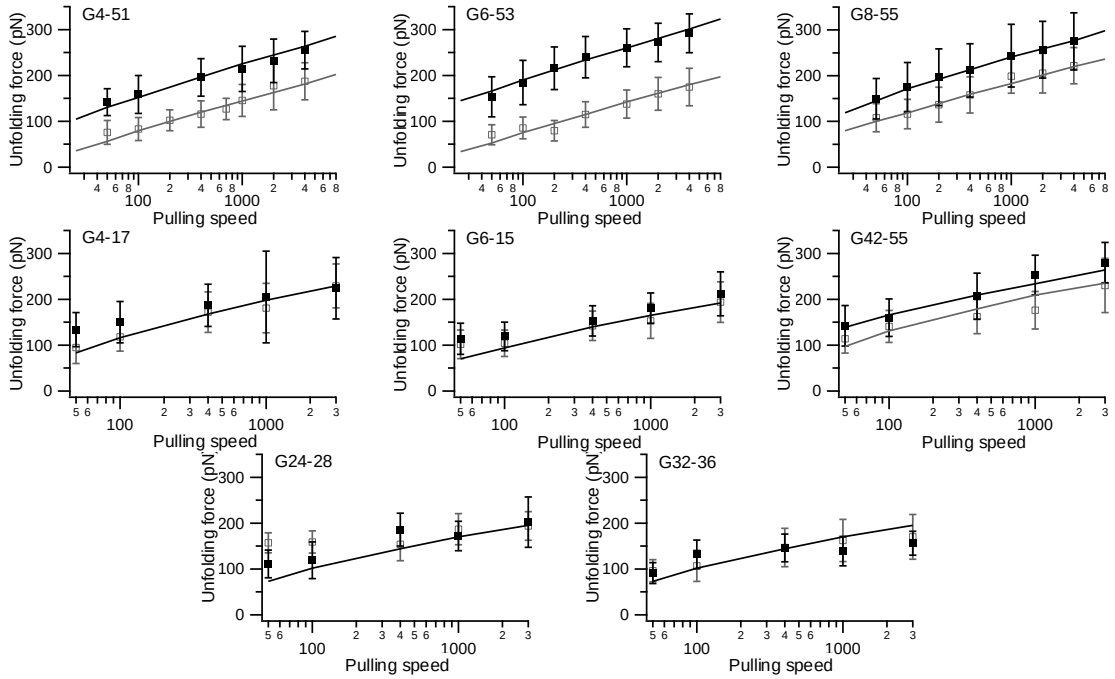

Figure 3.5 Pulling speed experiments involving bi-His mutants in the absence (gray) and presence (black) of 14.3 mM Ni^{2+}. In the presence of Ni^{2+} ions, the unfolding rate constants at zero force are decreased for mutants G4-51, G6-53, G8-55 and G42-55.

3.2 Discussion

3.2.1 The interface between the two force-bearing β-strands in the mechanical unfolding transition state of GB1

Bi-His mutants in the force-bearing β-strands 1and 4 show high φ_U^{M2+} values (0.7 – 1.3), suggesting that in the mechanical unfolding transition state, the bi-His sites across the two force-bearing strands are disrupted significantly and the binding affinity to Ni^{2+} at the transition state is significantly reduced. In the case of G6-53 and G8-55, the bi-His site is probably disrupted completely and no longer binds with Ni^{2+}. This conclusion is consistent with MD simulations[58, 59] that the key event in the mechanical unfolding of GB1 corresponds to the rupture of the force-bearing β-strands 1 and 4 and has been used to rationally enhance the mechanical stability of GB1[28].

It is of note that the φ_U^{M2+} value is higher than 1 for mutants G6-53 and G8-55. In principle, the highest φ_U^{M2+} should be 1. The observation of a φ_U^{M2+} value higher than 1 is probably due to errors associated with estimating the mechanical unfolding free energy change $\Delta\Delta G_{TS-N}$. It is known that the estimation of k_u^0 depends on Δx_u. Small variations in Δx_u may lead to major changes in k_u^0, resulting in errors in calculating the mechanical φ_U^{M2+} value.

3.2.2 The first and second β-hairpin in the mechanical unfolding transition state

Ni^{2+} binding does not lead to any change (either stabilizing or destabilizing) in the mechanical stability of G4-17 or G6-15, suggesting that the mechanical unfolding transition state has the same binding affinity to Ni^{2+} as the native state, giving rise to a zero $\varphi_U^{M\,2+}$ value for mutants G4-17 and G6-15. This result indicates that the first β-hairpin remains largely intact in the mechanical unfolding transition state.

In contrast, the bi-His mutant G42-55 in the second hairpin displays a different behavior. The binding of Ni^{2+} to the mutant G42-55 resulted in an increase in the mechanical unfolding force, giving rise to a $\varphi_U^{M\,2+}$ value of 0.39. This partial $\varphi_U^{M\,2+}$ value suggests that the structure around residues 42 and 55, which is at the end of the second β-hairpin, is partially disrupted in the mechanical unfolding transition state and shows a reduced binding affinity to Ni^{2+}. Since the G44-53 bi-His mutant does not bind with Ni^{2+} in the native state, G44-53 cannot, unfortunately, be used to probe the structural change of the whole second β-hairpin in the mechanical unfolding transition state.

3.2.3 The α-helix in the mechanical unfolding transition state

The binding of Ni^{2+} to bi-His mutants in the α-helix does not change the mechanical stability at all, giving rise to zero for the $\varphi_U^{M\,2+}$ value. This result suggests that the α-helix is intact in the mechanical unfolding transition state.

In summary, in the mechanical unfolding transition state of GB1, the α-helix and the first

β-hairpin remain largely intact. The mutation in the second β-hairpin shows an intermediate $\varphi_U^{M\,2+}$ value, suggesting that the second β-hairpin is partially disrupted and the bi-His site has a reduced binding affinity in the transition state. Mutations in the force-bearing β-strands 1 and 4 are close to one, indicating that the force bearing strands are deformed such that the bi-His metal chelation sites engineered across the two strands are completely disrupted and no longer bind with Ni^{2+} in the mechanical unfolding transition state (Figure 3.6). These results provide the first experimental picture of the mechanical unfolding transition state of GB1.

3.2.4 Comparison of structures of the unfolding transition state for mechanical unfolding and chemical unfolding

The folding and unfolding of GB1 has been studied extensively using classical ensemble chemical denaturation methods, and the structure of the unfolding transition state was mapped[60]. In the chemical unfolding transition state, the first hairpin is largely unstructured, whereas the second hairpin remains fully structured. The formation of the second hairpin is critical to reaching the transition state along the folding pathway. Moreover, it was found that the second hairpin is stable in isolation[60, 61]. This picture of the chemical unfolding transition state is drastically different from that of the mechanical unfolding. In the mechanical unfolding transition state, the second hairpin is partially unstructured and unravels first, while the first hairpin remains structured, revealing a sharp difference between the two transition state structures, and thus a difference between the two unfolding pathways. It is worth noting that during mechanical unfolding, it is the

more stable second hairpin that unravels first, again revealing the fact that mechanical and thermodynamic stability may not correlate with each other[43]. The reason underlying this interesting behavior is yet to be uncovered. It is likely that the interactions between the α-helix and the two terminal β-hairpins further modify the relative mechanical stability of the two hairpins.

3.2.5 Comparing single molecule AFM studies and MD simulations

The mechanical unfolding of GB1 has been simulated using MD simulations[58, 59, 62]. MD simulations predict that the forced unfolding of GB1 proceeds through two highly similar pathways[58, 59]. In the case of the first, the N- and C-terminal β-hairpins slide concurrently against each other along the α-helix; in the case of the second, the C-terminal β-hairpin detaches from the rest of the GB1 and unravels, leaving an intermediate state consisting of the intact N-terminal β-hairpin and α-helix. The differences between the two pathways are subtle, as the main difference lies in the timing when the contacts between the two terminal β-hairpins and the α-helix break. In both pathways, the contacts between the two force-bearing β-hairpins are disrupted first.

The structure of the mechanical unfolding transition state of GB1 mapped by our experimentally determined $\varphi_U^{M\,2+}$ is largely consistent with the MD simulation trajectories: the N-terminal β-hairpin and α-helix remain largely intact, while the contacts in the two force-bearing strands are completely disrupted.

The MD simulations also raised the possibility of an alternative interpretation of the partial $\varphi_U^{M\,2+}$ value observed for G42-55. We interpreted the this value observed for G42-

55 as an indication that the bi-His site 42-55 in the mechanical unfolding transition state was partially disrupted, leaving its with a lower binding affinity to Ni^{2+}, suggesting that the C-terminal β-hairpin is partially unstructured in the mechanical unfolding transition state. However, MD simulations predicted two different unfolding pathways[58], in which the rupture of the C-terminal β-hairpin occurs either simultaneously with or following the disruption of the contacts between strands 1 and 4. In this vein, the partial $\varphi_U^{M\,2+}$ value observed for G42-55 could be interpreted as a measure of the heterogeneity of the unfolding pathways, as originally put forward by Sosnick in developing Ψ value analysis[30, 32]. Since the mechanical stability of G42-55 shows distinct mechanical stability in the apo- or Ni^{2+} form, it is not possible to tune the mechanical stability continuously, unlike the case in chemical Ψ -value analysis. Thus, it is difficult to distinguish the two scenarios for the partial $\varphi_U^{M\,2+}$ value observed for G42-55. Nonetheless, the engineered metal chelation-based $\varphi_U^{M\,2+}$ value analysis demonstrated here provides an experimental means to map the mechanical unfolding transition state; moreover, it can be used as benchmarks for MD simulations, just as the Φ and $\tilde{\Psi}$ value analysis have been used to achieve a synergistic understanding of protein folding/unfolding mechanism by means of experiments and simulations.

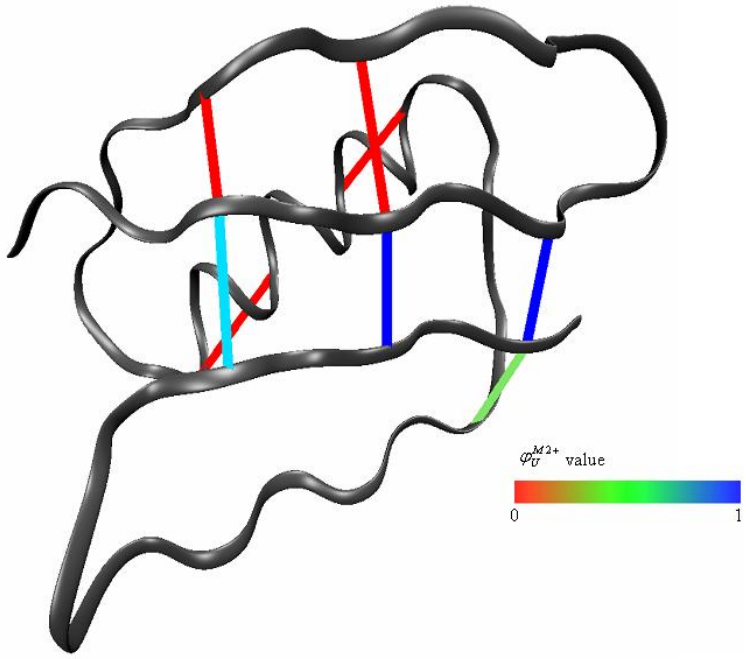

Figure 3.6 Mechanical φ_U^{M2+} values reveal the structure of mechanical unfolding transition state of GB1. In the mechanical unfolding transition state of GB1, the interface between the two force-bearing strands 1 and 4 is largely disrupted and the second β-hairpin is partially unstructured. In contrast, the first β-hairpin and the a-helix remain largely intact in the mechanical unfolding transition state.

Table 3.1 Summary of (i) bi-His mutant equilibrium denaturation, unfolding force, spontaneous unfolding rate constant at zero force in the absence and presence of Ni^{2+}; (ii) changes in thermodynamic stability, unfolding energy barrier ($\Delta\Delta G_{TS-N}$) for all bi-His mutants and (iii) bi-His mutant φ_U^{M2+}

Mutant	$D_{1/2}$(apo) (M)	$D_{1/2}(Ni^{2+})$ (M)	$\Delta\Delta G_{D-N}$ (kCal/mol)	Fu (apo) (pN)	Fu (Ni^{2+}) (pN)	Δx_u (apo) (nm)	k_u^0 (apo) (s^{-1})	Δx_u (Ni^{2+}) (nm)	k_u^0 (Ni^{2+}) (s^{-1})	$\Delta\Delta G_{TS-N}$ (kCal/mol)	ψ_U^{M2+}
G6-53	1.34	2.01	1.59	119±19	243±49	0.20	0.14	0.17	0.0071	1.79	1.13
G4-51	1.21	1.93	1.47	120±29	198±43	0.20	0.12	0.17	0.023	0.99	0.67
G8-55	2.21	2.41	0.36	160±38	219±57	0.20	0.029	0.17	0.014	0.44	1.22
G6-15	1.78	1.36	-1.04	142±33	140±31	0.20	0.07	0.20	0.07	~0	0
G4-17	2.36	3.10	1.48	177±48	187±47	0.17	0.07	0.17	0.07	~0	0
G42-55	1.96	2.74	1.39	160±37	207±50	0.17	0.05	0.17	0.02	0.54	0.39
G24-28	1.72	2.73	1.39	155±34	148±33	0.20	0.08	0.20	0.08	~0	0
G32-36	2.08	2.63	1.02	155±33	146±32	0.20	0.06	0.20	0.06	~0	0

Chapter 4 Mechanical stability enhancement by various divalent metal ions

4.1Results

4.1.1 Enhancing the mechanical stability of G6–53 by binding with Co^{2+}, Zn^{2+} and Cu^{2+} ions

The force-extension curve of apo form $(G6–53)_8$ is a characteristic sawtooth pattern. All force peaks, except the last one, correspond to the mechanical unfolding of the individual G6–53 domains in the polyprotein. After fitting the force-extension curves using worm-like-chain model, we found that the unfolding force peaks were equally spaced. The contour length increment (ΔL_c) was 18nm. The average unfolding force for $(G6–53)_8$ free of metal ions was 119 ±29 pN at a pulling speed of 400 nm/s. Cao et al. has demonstrated the Ni^{2+} could enhance G6-53 mechanical stability[28]; the force is almost doubles. To further investigate whether Co^{2+}, Zn^{2+} and Cu^{2+} can enhance the mechanical stability of G6–53, we carried out single molecular force measurements of $(G6–53)_8$ in the presence of 14.3 mM Co^{2+}, Zn^{2+} and Cu^{2+} ions, respectively. All the unfolding force peaks for G6–53 in the presence of these three metal ions were equally spaced, and the contour length increments identical to G6–53 in the absence of metal ions. The average unfolding force G6–53 in 14.3 mM Cu^{2+} is 234 ±40 pN, which is similar to that of G6-53 with Ni^{2+} ions. The binding of Co^{2+} ions led to the smallest force increase among these

three metal ions. The unfolding force changed to 195 ±58 pN. In the case of Zn^{2+} ions, the unfolding force increased to 211 ±44 pN. The different unfolding force for $(G6–53)_8$ with or without metal ions are tabulated in Table 4.1. These results clearly demonstrate that the binding of Co^{2+}, Zn^{2+} and Cu^{2+} ions to the metal chelation site enhances the mechanical stability of G6–53.

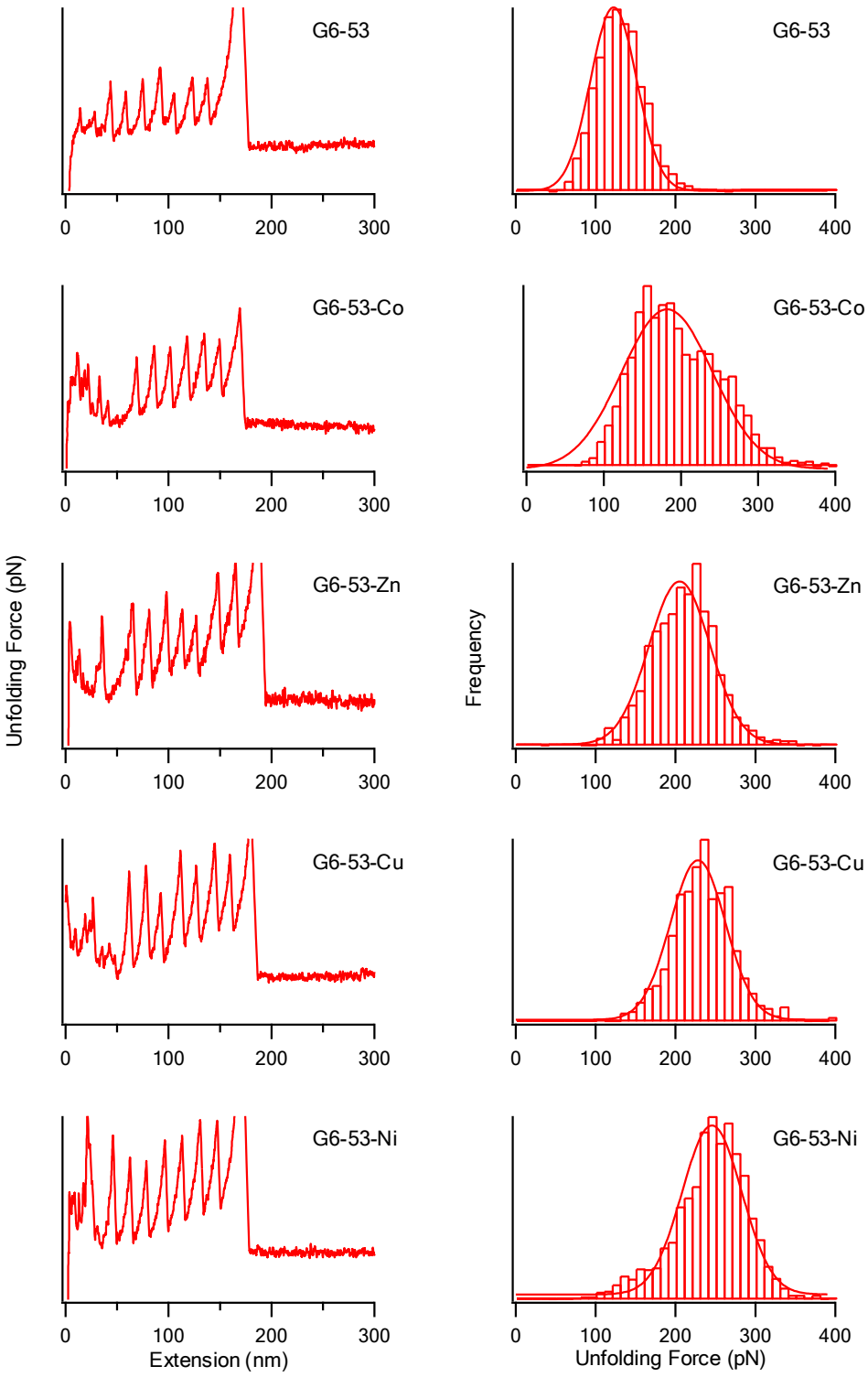

Figure 4.1 The force-extension curves and unfolding force histograms of G6-53 in the absence and presence of different metal ions. In the presence of metal ions, the mechanical unfolding force shifts towards higher forces.

4.1.2 Enhancing mechanical stability by increasing the unfolding free energy barrier

Preferential stabilization of the native state over the mechanical unfolding transition state increases the unfolding free energy barrier. This is an essential condition for enhancing mechanical stability as proved by Cao et al. using Ni^{2+} [28]. To quantify the increment of the unfolding free energy barrier following the binding of Co^{2+}, Zn^{2+} and Cu^{2+}, we conducted single molecule AFM stretching experiments on $(G6\text{-}53)_8$ with these three metal ions at different puling speeds. The unfolding force depends on the pulling speeds: the faster the pulling speed is, the greater the unfolding force. The mechanical unfolding rate constant at zero force and the distance between the native state and transition state were estimated by Monte Carlo simulation procedures[4, 41, 57]. The reproduced unfolding forces from the simulations were used to fitting the unfolding force distributions and their dependence on pulling speeds as shown in Figure 4.2. The unfolding distance 0.17 is applicable for $(G6\text{-}53)_8$ in the presence of all metal ions. The mechanical unfolding rate constants at zero force are different for each metal ion. Cu^{2+} and Ni^{2+} ions reduce k_u^0 to the same rate 0.0071 s^{-1}. With Zn^{2+} ions, k_u^0 is 0.015 s^{-1}. Co^{2+} ions have the least influence on k_u^0, reducing it to 0.025 s^{-1}. The enhancement of the unfolding free energy barrier with metal chelation is defined as $-RT\ln[k_u^0(metal-bound)/k_u^0(metal-free)]$, where R is the gas constant, T the absolute temperature. From this formula, we can determine the $\Delta\Delta G_{TS-N}$ in $(G6\text{-}53)_8$ after chelating the four metal ions. The $\Delta\Delta G_{TS-N}$ indicates that all the metal ions selectively enhanced the energy barrier for the rate-limiting step. The mechanical unfolding rate constants at zero force, the unfolding distance and

the $\Delta\Delta G_{TS-N}$ are summarized in Table 4.1.

It is worthy to note that, the unfolding distance of G6-53 in the absence of metal ions was 0.20nm. The reduced unfolding distance following the binding of the metal ions also contributed to enhancing of the mechanical stability.

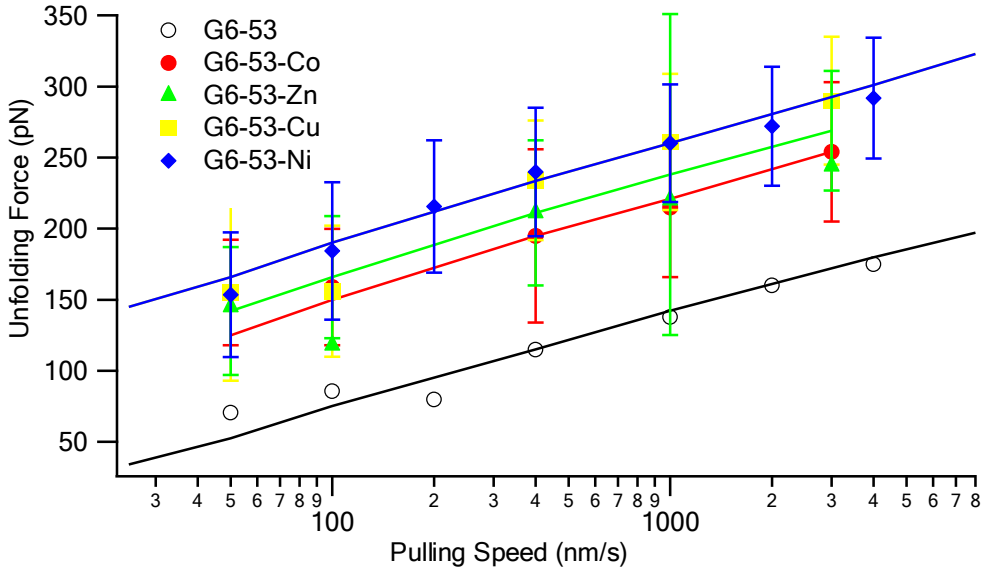

Figure 4.2 Speed dependence of the mechanical unfolding forces of G6-53 in the absence and presence of metal ions. In the presence of metal ions, the unfolding distance decreased to 0.17 nm. The unfolding rate constants at zero force varied from 0.0071 to 0.025 s^{-1}.

4.1.3 Reversibility of enhancement of mechanical stability by metal ion binding

The mechanical stability enhancement of G6-53 results from the binding of metal ions to the metal chelation site. As is well known, EDTA (ethylenediaminetetraacetic acid) has a high metal ion binding affinity. If this competitive-binding agent is added to the protein solution containing metal ions, the metal ions will be dissociated from the bi-his site.

Thus, this allows us to modulate the mechanical stability of G6-53 in a convenient way. This has been proved to be true in the case of Ni^{2+}. We further studied the influence of EDTA on G6-53 with Co^{2+}, Zn^{2+} and Cu^{2+}. As shown in figure 4.3, after addition of EDTA, all the three mechanical unfolding forces of G6-53 in the presence of Co^{2+}, Zn^{2+} and Cu^{2+} fell to ~120 pN. This demonstrates that the reversibility of the binding and unbinding process. The metal ions and EDTA are utilized to selectively adjust the mechanical stability of G6-53 between the two distinct mechanical forms. The reversible modulation offers the possibility to modulate the mechanical stability using environmental stimuli.

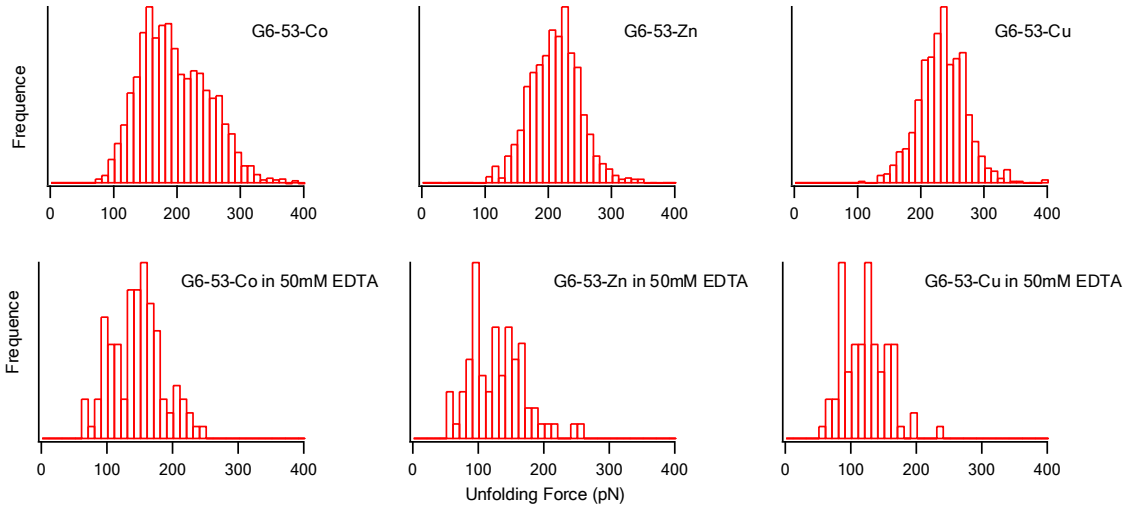

Figure 4.3 Reversible regulation of the mechanical stability of G6–53 by the binding of metal ions or EDTA. The top ones represent the unfolding force histograms in the presence of Co^{2+}, Zn^{2+} and Cu^{2+}, respectively. Upon adding 50mM EDTA to the solution, all the unfolding forces of metal bound form G6-53 shifted back to the unfolding forces of their apo form.

Table 4.1 Summary of unfolding force, unfolding distance and unfolding rate constant at zero force for G6-53 in the absence and presence of metal ions and changes in unfolding energy barrier ($\Delta\Delta G_{TS-N}$)

mutant	Unfolding Force ± SD (pN)	Δx_u (nm)	k_u^0 (s^{-1})	$\Delta\Delta G_{TS-N}$ (kCal/mol)
G6-53	119 ±29	0.20	0.14	
G6-53-Co	195 ±58	0.17	0.025	1.02
G6-53-Zn	211 ±44	0.17	0.015	1.32
G6-53-Cu	234 ±40	0.17	0.0071	1.79
G6-53-Ni	243 ±49	0.17	0.0071	1.79

4.2 Discussion

4.2.1 Using engineered metal chelation to modulate the mechanical stability of proteins

Previous single molecule AFM studies have revealed that metal chelation can enhance the mechanical stability of proteins[28, 55]. This approach not only enhances the mechanical stability of simple two-state proteins, like GB1, but is also applicable to proteins with a complex unfolding behavior[55]. Here we further demonstrated that, using the same

approach, it is even possible to enhance the mechanical stability by adding various metal ions. All four metal ions significantly increased the mechanical stability. Thus, the engineered metal chelation approach is not limited to particular proteins or specific metal ions. It is a general approach to rationally enhance the mechanical stability of proteins.

4.2.2 Reversibility of modulation mechanical stability

One of the major advantages of using metal ions to enhance mechanical stability is the reversibility of the process. Addition of EDTA reduces the unfolding forces back to their apo form. The unfolding force difference between the apo and metal bound form proteins is enormous. In the presence of metal ions, the unfolding force is almost doubled. Reversibility offers the possibility of treating the protein as a switch. Thus, we can use environmental stimuli to modulate the mechanical stability of the protein in its two distinct mechanical forms

4.2.3 Using various metal ions to fine tune the mechanical stability of proteins

Different metal ions enhance mechanical stability to different degrees, the unfolding force ranging from 195 pN to 243 pN. This is applicable to controlling the enhancement of mechanical stability in an additional way. The resultant unfolding force difference between Co^{2+} and Zn^{2+} or Zn^{2+} and Cu^{2+} is ~ 20 pN. Thus, various metal ions can be utilized to fine tune the mechanical stability of proteins

Chapter 5 Summary and future work

5.1 Summary of work

Single molecule AFM is a powerful technique affording the opportunity to understand the mechanical properties of proteins at the level of a single molecule. Metal ions are crucial to the function of many protein machineries inside cells[21-24]. They participate in catalytic cycles of enzymes, mediate the protein–ligand interactions, and maintain the structure of proteins. In this thesis, we employed bi-His metal binding sites to probe the mechanical unfolding transition state of a protein and rationally enhance protein mechanical stability.

The transition state cannot be trapped and detected by the usual structural methods because of its high free energy. It remains a challenging task and research focus. In Chapter 3, we directly probed the mechanical unfolding transition state structure of protein GB1. The results demonstrate that the contacts between the force-bearing strands 1 and 4 are largely disrupted at the transition state, whereas the first β-hairpin and α-helix were largely intact. The second hairpin was partially disrupted. These results are in close agreement with, and provide a benchmark for, MD simulations.

The mechanical stability is critical for the overall mechanical properities of elastomeric proteins. Elastomeric proteins provide tissues with extensibility, elasticity, and mechanical strength. In Chapter 4, we enhanced the mechanical stability of G6-53 with different metal ions. We demonstrated that all four divalent metal ions, Ni^{2+}, Co^{2+}, Zn^{2+} and Cu^{2+}, enhance the mechanical stability of G6-53 to different degrees. Because this process is completely reversible, the protein can be treated like a switch. Moreover, the

resultant unfolding force difference between Co^{2+} and Zn^{2+} or Zn^{2+} and Cu^{2+} is ~ 20 pN. Thus, various metal ions can be used to fine tune the mechanical stability of proteins.

5.2 Future work

As we discussed in 1.2.2, the Arnold group enhanced the thermodynamic stability of a protein by two classes of metal ions: the kinetically labile and substitution-inert metal ions. The former preferentially bind to the native rather than the denatured state to stabilize the protein. The latter crosslink the protein like a disulfide bond.

We have investigated the influence of kinetically labile metal ions, Ni^{2+}, Co^{2+}, Zn^{2+} and Cu^{2+} on the mechanical stability of G6-53. They bind preferentially to the folded protein rather than the transition state to enhance the mechanical stability.

Future studies might investigate the influence of substitution-inert metal ions on the mechanical stability of proteins. These ions remain bound when the protein unfolds like a disulfide bond. Typically, the force to break a covalent bond is about 1000 pN[63]. This force is higher than most of proteins studied so far. The next step would be to study the mechanical stability of proteins in the presence of substitution-inert metal ions.

References

1. G. Binnig, C. F. Quate and C. Gerber, *Physical Review Letters*, 1986, **56**, 930-933.
2. O. Marti, B. Drake and P. K. Hansma, *Appl. Phys. Lett.*, 1987, **51**, 484-486.
3. E. L. Florin, V. T. Moy and H. E. Gaub, *Science*, 1994, **264**, 415-417.
4. M. Carrion-Vazquez, A. F. Oberhauser, S. B. Fowler, P. E. Marszalek, S. E. Broedel, J. Clarke and J. M. Fernandez, *Proc. Natl. Acad. Sci. U. S. A.*, 1999, **96**, 3694-3699.
5. M. Rief, F. Oesterhelt, B. Heymann and H. E. Gaub, *Science*, 1997, **275**, 1295-1297.
6. B. D. Sattin, A. E. Pelling and M. C. Goh, *Nucleic Acids Res.*, 2004, **32**, 4876-4883.
7. T. Strunz, K. Oroszlan, R. Schafer and H. J. Guntherodt, *Proc. Natl. Acad. Sci. U. S. A.*, 1999, **96**, 11277-11282.
8. A. Noy, D. V. Vezenov, J. F. Kayyem, T. J. Meade and C. M. Lieber, *Chem. Biol.*, 1997, **4**, 519-527.
9. K. A. Walther, J. Brujic, H. B. Li and J. M. Fernandez, *Biophys. J.*, 2006, **90**, 3806-3812.
10. M. Rief and H. Grubmuller, *ChemPhysChem*, 2002, **3**, 255-261.
11. P. E. Marszalek, A. F. Oberhauser, Y. P. Pang and J. M. Fernandez, *Nature*, 1998, **396**, 661-664.
12. E.-L. Florin, A. Pralle, J. K. Heinrich H 枚 rber and E. H. K. Stelzer, *Journal of Structural Biology*, 1997, **119**, 202-211.
13. A. Ashkin, J. M. Dziedzic, J. E. Bjorkholm and S. Chu, *Opt. Lett.*, 1986, **11**, 288-290.
14. M. Rief, H. Clausen-Schaumann and H. E. Gaub, *Nat. Struct. Biol.*, 1999, **6**, 346-349.
15. M. Rief, M. Gautel, F. Oesterhelt, J. M. Fernandez and H. E. Gaub, *Science*, 1997, **276**, 1109-1112.
16. C. Bustamante, J. F. Marko, E. D. Siggia and S. Smith, *Science*, 1994, **265**, 1599-1600.
17. J. F. Marko and E. D. Siggia, *Macromolecules*, 1994, **27**, 981-988.
18. G. I. Bell, *Science*, 1978, **200**, 618-627.
19. E. Evans and K. Ritchie, *Biophys. J.*, 1997, **72**, 1541-1555.
20. E. Evans and K. Ritchie, *Biophys. J.*, 1999, **76**, 2439-2447.
21. R. H. Holm, P. Kennepohl and E. I. Solomon, *Chemical Reviews*, 1996, **96**, 2239-2314.
22. D. W. Christianson and J. D. Cox, *Annu. Rev. Biochem.*, 1999, **68**, 33-57.
23. T. Dudev and C. Lim, in *Annual Review of Biophysics*, Annual Reviews, Palo Alto, Editon edn., 2008, vol. 37, pp. 97-116.
24. C. J. Wilson, D. Apiyo and P. Wittung-Stafshede, *Q. Rev. Biophys.*, 2004, **37**, 285-314.
25. S. S. Suh, B. L. Haymore and F. H. Arnold, *Protein Eng.*, 1991, **4**, 301-305.
26. J. T. Kellis, R. J. Todd and F. H. Arnold, *Bio-Technology*, 1991, **9**, 994-995.
27. A. Muheim, R. J. Todd, D. R. Casimiro, H. B. Gray and F. H. Arnold, *J. Am. Chem. Soc.*, 1993, **115**, 5312-5313.
28. Y. Cao, T. Yoo and H. B. Li, *Proc. Natl. Acad. Sci. U. S. A.*, 2008, **105**, 11152-11157.
29. J. N. Higaki, B. L. Haymore, S. Chen, R. J. Fletterick and C. S. Craik, *Biochemistry*, 1990, **29**, 8582-8586.
30. B. A. Krantz and T. R. Sosnick, *Nat. Struct. Biol.*, 2001, **8**, 1042-1047.
31. B. A. Krantz, R. S. Dothager and T. R. Sosnick, *J. Mol. Biol.*, 2004, **337**, 463-475.
32. T. R. Sosnick, B. A. Krantz, R. S. Dothager and M. Baxa, *Chemical Reviews*, 2006, **106**, 1862-1876.
33. A. M. Gronenborn, D. R. Filpula, N. Z. Essig, A. Achari, M. Whitlow, P. T. Wingfield and G. M. Clore, *Science*, 1991, **253**, 657-661.
34. A. I. Bartlett and S. E. Radford, *Nature Structural & Molecular Biology*, 2009, **16**, 582-588.
35. A. R. Fersht and V. Daggett, *Cell*, 2002, **108**, 573-582.
36. J. N. Onuchic, Z. LutheySchulten and P. G. Wolynes, *Annual Review of Physical Chemistry*, 1997, **48**, 545-600.
37. Y. Cao, K. S. Er, R. Parhar and H. B. Li, *ChemPhysChem*, 2009, **10**, 1450-1454.
38. A. S. Tatham and P. R. Shewry, *Trends in Biochemical Sciences*, 2000, **25**, 567-571.
39. J. Gosline, M. Lillie, E. Carrington, P. Guerette, C. Ortlepp and K. Savage, *Philosophical Transactions of the Royal Society of London Series B-Biological Sciences*, 2002, **357**, 121-132.
40. B. L. Smith, T. E. Schaffer, M. Viani, J. B. Thompson, N. A. Frederick, J. Kindt, A. Belcher, G. D. Stucky, D. E. Morse and P. K. Hansma, *Nature*, 1999, **399**, 761-763.
41. A. F. Oberhauser, P. E. Marszalek, H. P. Erickson and J. M. Fernandez, *Nature*, 1998, **393**, 181-

185.
42. S. Labeit and B. Kolmerer, *Science*, 1995, **270**, 293-296.
43. H. B. Li, W. A. Linke, A. F. Oberhauser, M. Carrion-Vazquez, J. G. Kerkviliet, H. Lu, P. E. Marszalek and J. M. Fernandez, *Nature*, 2002, **418**, 998-1002.
44. G. Lee, K. Abdi, Y. Jiang, P. Michaely, V. Bennett and P. E. Marszalek, *Nature*, 2006, **440**, 246-249.
45. B. Bullard, T. Garcia, V. Benes, M. C. Leake, W. A. Linke and A. F. Oberhauser, *Proc. Natl. Acad. Sci. U. S. A.*, 2006, **103**, 4451-4456.
46. M. Rief, J. Pascual, M. Saraste and H. E. Gaub, *J. Mol. Biol.*, 1999, **286**, 553-561.
47. D. Sharma, O. Perisic, Q. Peng, Y. Cao, C. Lam, H. Lu and H. B. Li, *Proc. Natl. Acad. Sci. U. S. A.*, 2007, **104**, 9278-9283.
48. S. P. Ng, K. S. Billings, T. Ohashi, M. D. Allen, R. B. Best, L. G. Randles, H. P. Erickson and J. Clarke, *Proc. Natl. Acad. Sci. U. S. A.*, 2007, **104**, 9633-9637.
49. A. Borgia, A. Steward and J. Clarke, *Angewandte Chemie-International Edition*, 2008, **47**, 6900-6903.
50. D. Sharma, Y. Cao and H. B. Li, *Angewandte Chemie-International Edition*, 2006, **45**, 5633-5638.
51. S. R. K. Ainavarapu, L. Y. Li, C. L. Badilla and J. M. Fernandez, *Biophys. J.*, 2005, **89**, 3337-3344.
52. M. Bertz and M. Rief, *J. Mol. Biol.*, 2008, **378**, 447-458.
53. Y. Cao, M. M. Balamurali, D. Sharma and H. B. Li, *Proc. Natl. Acad. Sci. U. S. A.*, 2007, **104**, 15677-15681.
54. Y. Cao, T. Yoo, S. L. Zhuang and H. B. Li, *J. Mol. Biol.*, 2008, **378**, 1132-1141.
55. S. L. Zhuang, Q. Peng, Y. Cao and H. B. Li, *J. Mol. Biol.*, 2009, **390**, 820-829.
56. Y. Cao and H. B. Li, *Nature Materials*, 2007, **6**, 109-114.
57. M. Rief, J. M. Fernandez and H. E. Gaub, *Physical Review Letters*, 1998, **81**, 4764-4767.
58. A. V. Glyakina, N. K. Balabaev and O. V. Galzitskaya, *Journal of Chemical Physics*, 2009, **131**.
59. A. V. Glyakina, N. K. Balabaev and O. V. Galzitskaya, *Biochemistry-Moscow*, 2009, **74**, 316-328.
60. E. L. McCallister, E. Alm and D. Baker, *Nat. Struct. Biol.*, 2000, **7**, 669-673.
61. F. J. Blanco, G. Rivas and L. Serrano, *Nat. Struct. Biol.*, 1994, **1**, 584-590.
62. P. C. Li and D. E. Makarov, *Journal of Physical Chemistry B*, 2004, **108**, 745-749.
63. M. K. Beyer and H. Clausen-Schaumann, *Chemical Reviews*, 2005, **105**, 2921-2948.